



HAL
open science

Sources of stationary and low-frequency magnetic fields in inhabited areas

Nicolas Petit

► **To cite this version:**

Nicolas Petit. Sources of stationary and low-frequency magnetic fields in inhabited areas. [Research Report] Centre Automatique et Systèmes MINES ParisTech. 2015. hal-01220593

HAL Id: hal-01220593

<https://minesparis-psl.hal.science/hal-01220593>

Submitted on 26 Oct 2015

HAL is a multi-disciplinary open access archive for the deposit and dissemination of scientific research documents, whether they are published or not. The documents may come from teaching and research institutions in France or abroad, or from public or private research centers.

L'archive ouverte pluridisciplinaire **HAL**, est destinée au dépôt et à la diffusion de documents scientifiques de niveau recherche, publiés ou non, émanant des établissements d'enseignement et de recherche français ou étrangers, des laboratoires publics ou privés.

Sources of stationary and low-frequency magnetic fields in inhabited areas

Nicolas Petit
Centre Automatique et Systèmes
MINES ParisTech

This document exposes some of the sources of stationary and low-frequency magnetic fields that can be found in inhabited areas.

One of the strongest magnetic field that one can observe is the Earth's magnetic field with an average of $48 \mu\text{T}$ in Central Europe. However, living in the 21st century, it is one of the few magnetic fields originating from a natural source. Modern life involves innumerable artificial sources of (electro-)magnetic fields, ranging from simple refrigerator magnets to wireless LAN. These "man-made" fields are often linked to electric currents respectively to electric fields and occur in a frequency domain from 0 Hz to several GHz [18].

We consider here magnetometers working at relatively low frequencies, that is to say less than 500 Hz. In addition, only magnetic fields greater than

$$3 \cdot \sigma_{noise} = 1.35 \mu\text{T}$$

can be clearly distinguished from noise of the embedded magnetometers [20].

1 The Geomagnetic Field

The geomagnetic field surrounding and penetrating the Earth is primarily produced in its interior. About 95 percent can be attributed to the convection and rotation of electrically conductive materials, particularly iron, in the liquid outer Earth's core. The convection currents result from temperature differences and chemical potential differences between the Earth's surface and its inner core, whereas the rotation is caused by the Coriolis force originating from the planetary rotation [10]. According to the dynamo theory [5], the geomagnetic field is induced and stabilised by the electric current generated by the movement of the electrically conductive iron melt in the magnetic field itself.

The remaining 5 percent of the geomagnetic field mainly have their origin in electric currents in the ionosphere; the magnetisation of the outer layers of the Earth only have a minor impact [10].

The geomagnetic field on the Earth's surface can be approximated as a dipole field, resembling to the magnetic field of a simple bar magnet. With increasing distance to the surface the number of magnetic disturbances rises so that the dipole field is distorted.

At present the axis of this dipole is tilted by around $11\hat{\text{A}}^\circ$ to the Earth's rotation axis. It should be noted that the magnetic force lines point towards the Earth in the Northern Hemisphere and into outer space in the Southern Hemisphere. Consequently, this means that the geographical North is close to the South Magnetic Pole and vice versa, see figure 1.

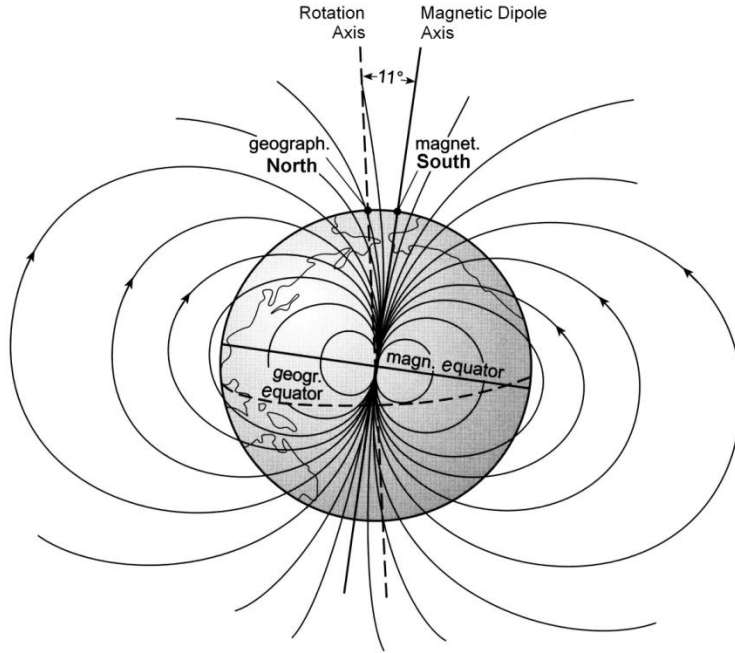


FIGURE 1 – Schematic representation of the Earth's magnetic field [2]

However, the Earth's magnetic field is going to be considered as stationary in the following, it is strictly speaking only quasi-stationary. It faces irregular short and long-term changes caused by solar winds, magnetic storms, changes in the ionosphere, incidents in the Earth's core or crust [10]. Moreover, the geomagnetic field has undergone a continuous reduction in field strength over at least the past century. This could possibly indicate that the magnetic field is about to reverse itself within the next thousand years; an event that on average takes place every 500.000 years [10].

1.1 Solar Quiet Variation

Figure 2 illustrates the variation and the rate of change of the Earth's magnetic field over the course of a calm day at the survey station of Chateau-la-Forêt, which is located approximately 100 km south of Paris. Subfigure (a) displays the deviation from the calculated mean of the three components of the magnetic field in nT. B_x points northwards, B_y eastwards and B_z points vertically downwards. The mean, stated in the right margin, is calculated individually for each vector component over the observed period of 24 hours. The sampling rate is 1 per minute. F , which is shown in the fourth diagram, denotes the vector sum of the three components. The corresponding rate of change of B_x , B_y and B_z in nT/min is shown in subfigure (b).

The course of the one-minute variation curve, especially of the horizontal components, shows a very characteristic daily-periodic fluctuation of the geomagnetic field. It is called the solar quiet course, which bears a simple reason : this kind of variation of the Earth's magnetic field can only be detected on magnetically quiet days, that is on solar wind free days.

The reason for the solar quiet variation lies about 90 to 130 km above the Earth's surface, in the ionosphere. This part of the Earth's atmosphere contains large quantities of free elec-

trons and ions and consists of several layers. Of particular interest for the geomagnetic field is the so-called E(lectrical)-layer that emerges on the sunlit side of the Earth and nearly disappears after sundown. Currents of electrically conducting, ionised gases within this layer induce electric currents and thus magnetic fields. As the E-layer reaches its maximum extension and ionisation at noon, the influence on the geomagnetic field is most pronounced during that time of the day [12], [14].

As can be seen from figure 2, the solar quiet variation does not exceed a rate of change of ± 1.5 nT/min on this particular day. But even on less quiet days this value only increases to about ± 5 nT/min.

1.2 Solar Disturbed Variation

The geomagnetic field is not only facilitating navigation and orientation, but also fulfils the essential function of protecting the Earth against solar winds and cosmic radiation. The solar wind is a constant stream of protons, electrons, alpha particles and neutrons released by the Sun. It massively deforms the geomagnetic field at a distance of several Earth's radii. During a magnetic storm, caused by Sun eruptions, the plasma stream from the Sun is strong enough to enter the upper layers of the Earth's atmosphere. The interactions with the particles in the ionosphere induce electric currents and subsequently relatively fast variations of the magnetic field [10]. Figure 3 - identically structured as figure 2 - shows the effects on the geomagnetic field of a strong solar storm that occurred in autumn 2003. Just as the solar quiet variation, which can also be attributed to the ionosphere, mainly the two horizontal components are affected. The main differences between figure 2 and figure 3 not only lies in the course of the curves, but also in the scales. For example, the one-minute variation of the B_y -component ranges between 400 nT and -600 nT on magnetic storm day, whereas the magnetic field varies between 20 nT and -30 nT on a solar quiet day.

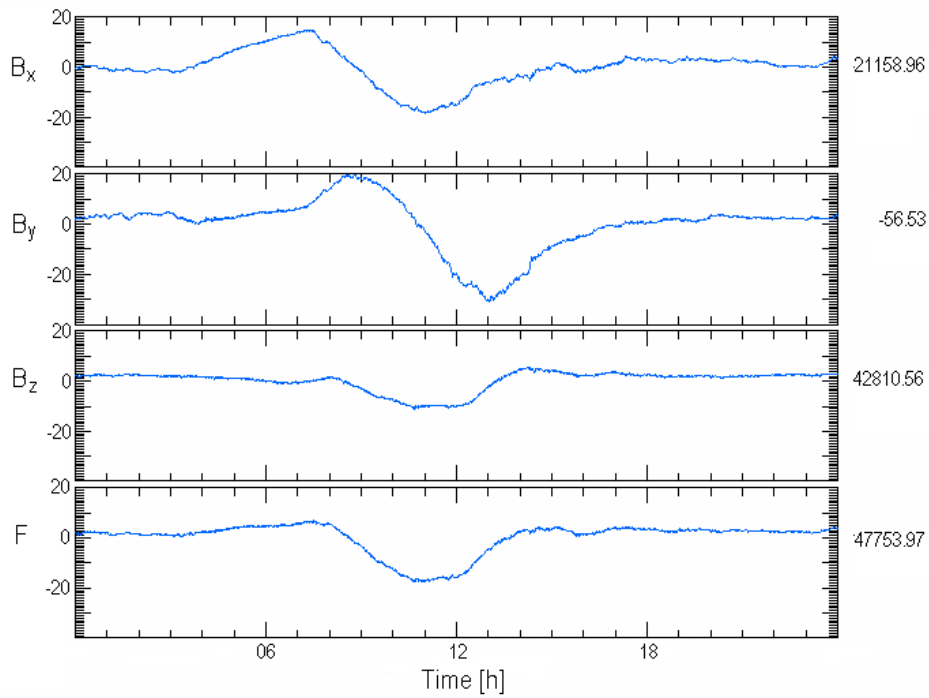
However, even the peak between 6am and 7am, where the magnetic field changes about 800 nT within an hour, could not be distinguished from the noise of the measurement device. As a conclusion we can state that *the geomagnetic field can safely assumed to be stationary.*

2 Electric Appliances and Installations

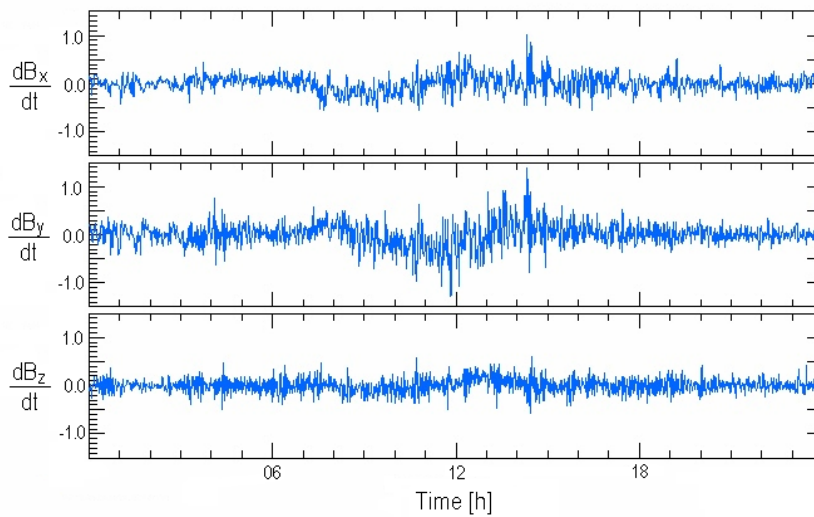
Inevitably encountering the geomagnetic field, we additionally face a great number of electric-current-induced magnetic fields in daily life. These result from the electric devices, which surround us, and the electric installations supplying them.

2.1 Electric Appliances

Households, offices and small businesses in Europe are usually supplied by the low voltage distribution grid with 400 V, 50 Hz three-phase current. From the grid connection point the current is then distributed by alternating (AC) and three-phase current cables to the various power-points and consumers within the building. Power current consumers, such as a cooker or electric heating, are provided with full three-phase current, whereas weak consumers are only supplied with one of the three phases. To the latter belong computers, screens, lights and so forth. All these electric devices create stationary and alternating (electro-)magnetic fields induced by the electric current. Especially appliances with high power consumption and those containing solenoids/transformers or an electric motor create strong magnetic fields.

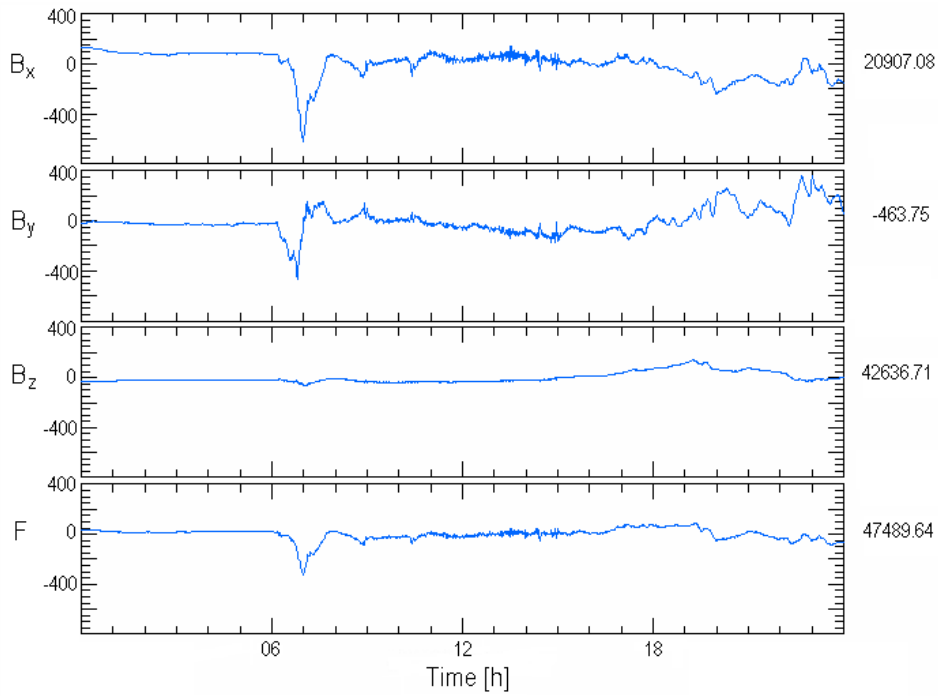


(a) One minute variation in nT

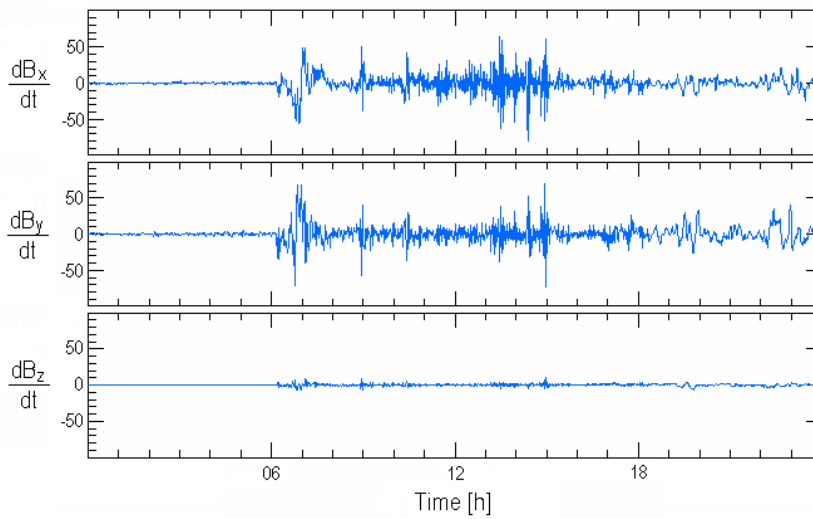


(b) Rate of change in nT/min

FIGURE 2 – Geomagnetic field at the survey station of Chambon-la-Forêt on a calm day (11th of November, 2012), data provided by www.intermagnet.org



(a) One minute variation in nT



(b) Rate of change in nT/min

FIGURE 3 – Geomagnetic field at the survey station of Chambon-la-Forêt on a magnetic storm day (29th of October, 2003), data provided by www.intermagnet.org

As an example, figure 4, 5 and 6 display the time courses of the magnetic fields induced by a laptop battery¹, a power supply unit (PSU) and a conventional filament lamp. The always-present stationary part of the magnetic field in the fixed test measuring point was vectorially eliminated. As the measurements were performed indoors, this is the geomagnetic field distorted in an unknown manner by mostly metal construction parts. It was calculated as the average of a 10 minute measurement period, in order to rule out possible time-dependent magnetic disturbance sources. However, for the actual measurements of the different electric devices it was not possible to filter external time-dependant influences, such as the Parisian metro.

The magnetic field of the laptop battery shown in figure 4 is clearly the field induced by a *direct current*. The absolute value remains between the borders of 34 and 36 μT , the high-frequency share can be attributed to the measurement noise. As the Y-component is constant, the slight changes in the *x*- and *z*-component are most likely to be caused by an external source. On the contrary, figure 5 looks very different. It shows the magnetic field of a laptop PSU, containing a transformer and a rectifier. The magnetic field, both absolute value and component-wise, is characterised by a pulsed course resulting from short charging phases. In these phases the field is oscillating because the measurements were taken at the AC supply side of the PSU. The filament lamp, which is also supplied with alternating current, creates a similar field depicted in figure 6. But, it is continuously alternating, that is to say the magnetic field does not have an additional overlaid time-course profile. The time section was chosen very small in order to reveal the oscillations; it should be noted that measurements over a wider time span have beats.

We conducted measurements for many other electric appliances, inter alia screens, phones, cold and warm light lamps, a drilling machine, a vacuum cleaner, a fan heater etc. In favour of a concise description of my work only the previously discussed are displayed because they show characteristic curve shapes: electric appliances create either stationary (figure 4), pulsating (figure 5) or alternating magnetic fields (figure 6). Naturally, depending on their circuit diagram, some devices also create mixed forms. For example, the magnetic field of the propulsion chain of a drilling machine, shown in figure 7, has an alternating and a pulsating contribution.

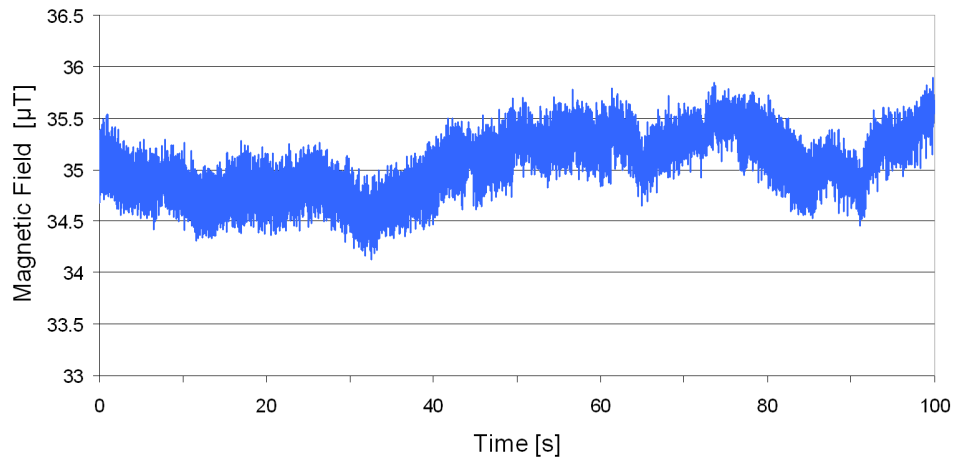
In order, nevertheless, to get an overview of the magnetic field of the most common electric appliances, the average values published by the *Deutsches Bundesamt für Strahlenschutz*², are listed in table 1.

But, table 1 also shows that - and our measurements have confirmed this - the magnetic field rapidly decreases as the distance to the emitter increases. For example, *an average computer cannot be detected by a typical magnetometer at a distance of 1 m*. Why is that? Common electric appliances contain all sorts of electrical parts: inductors, capacitors, transformers, rectifiers, electric motors, heater spirals, batteries and so forth. Regarding their magnetic fields these very different components can be reduced to a few basic sources, namely the current-carrying wire, the static and the oscillating dipole. E.g. the magnetic field induced by a solenoid passed through by a direct current is similar to the one of a static dipole. However, most of the above mentioned electrical parts have relatively small dimensions. According to [19], this is why their radiation behaviour resembles the static or oscillating dipole, which is characterised by a magnetic field loss proportional to $1/r^3$; r denotes the distance. Hence, magnetic fields emitted by common electrical devices are only measurable at very small distances.

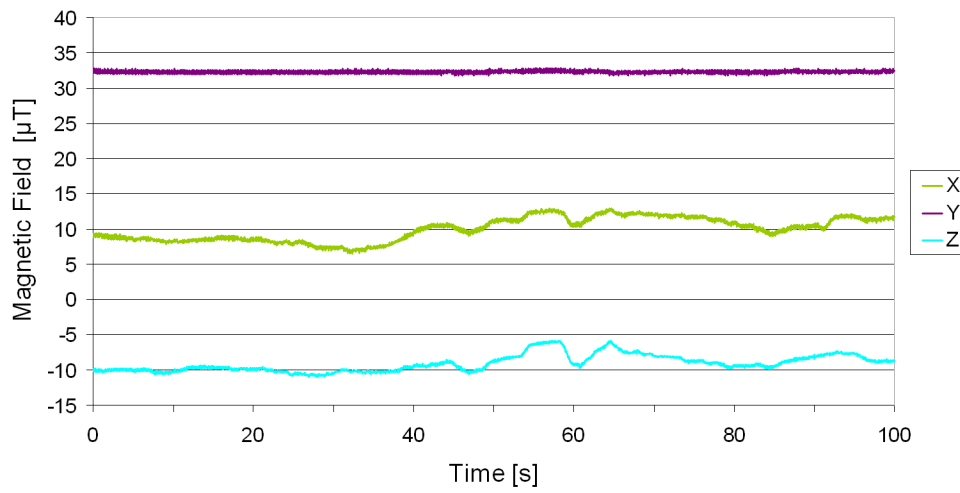
At this point, we can conclude that electrical appliances found in households and offices

1. while CPU in usage

2. German Federal Office for Radiation Protection

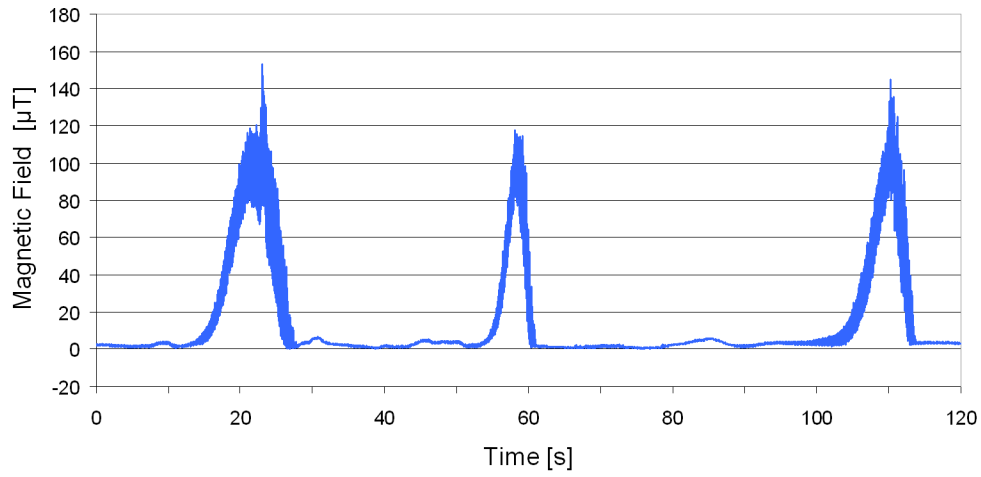


(a) Absolute value of the magnetic field

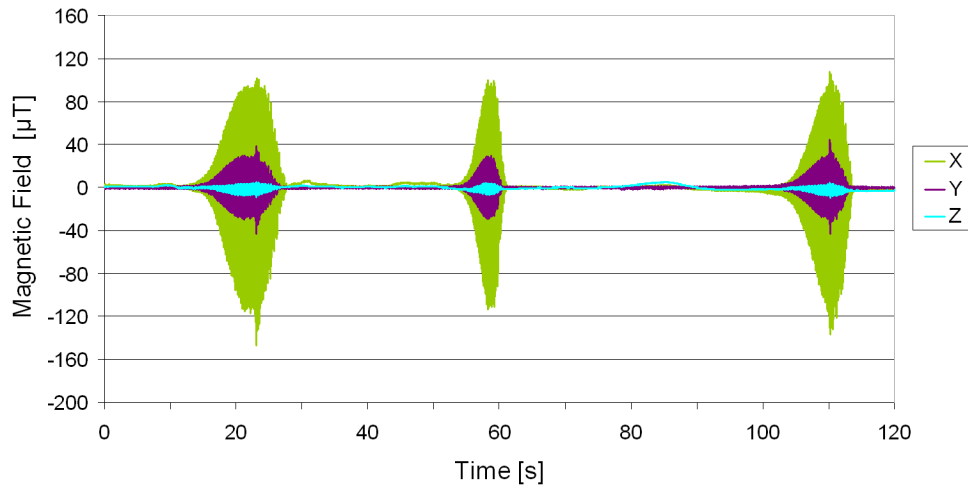


(b) Component-wise representation of the magnetic field

FIGURE 4 – Time course of the magnetic field measured at a distance of 1 cm of a laptop battery (specification in Appendix)

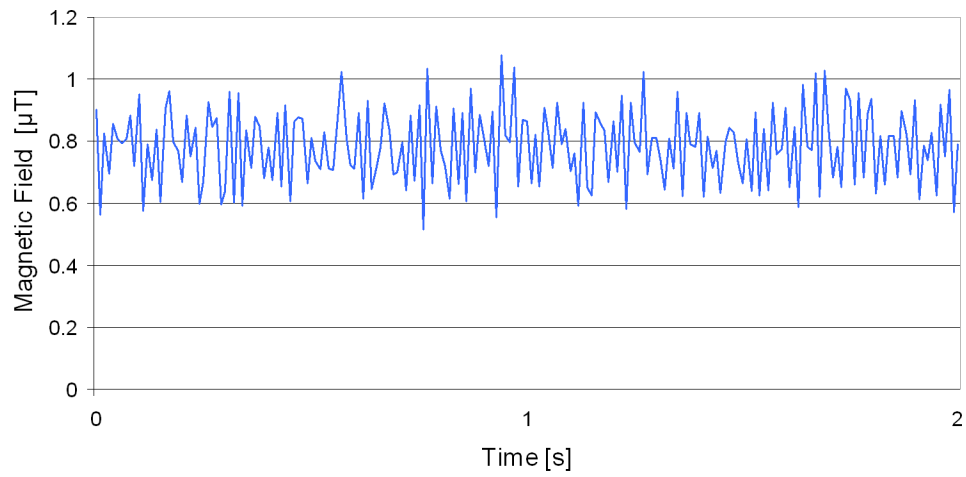


(a) Absolute value of the magnetic field

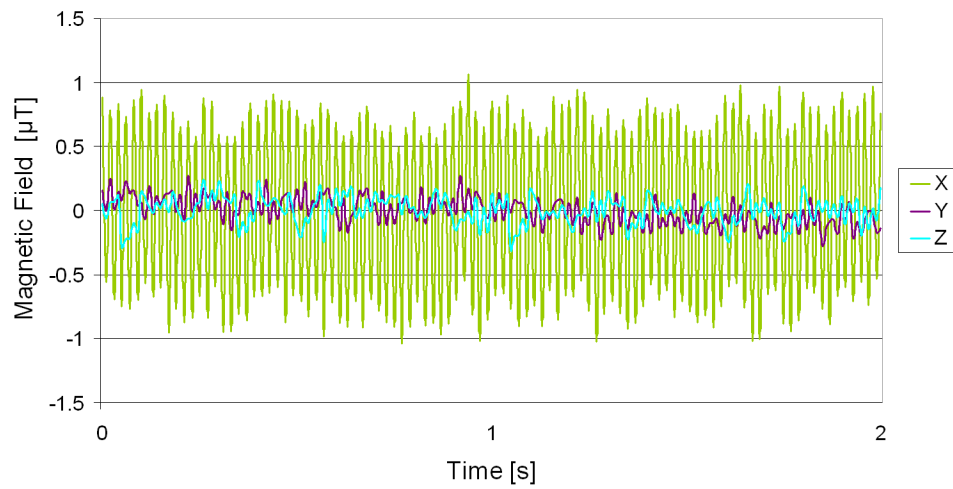


(b) Component-wise representation of the magnetic field

FIGURE 5 – Time course of the magnetic field measured at a distance of 1 cm of a power supply unit (specification in Appendix)

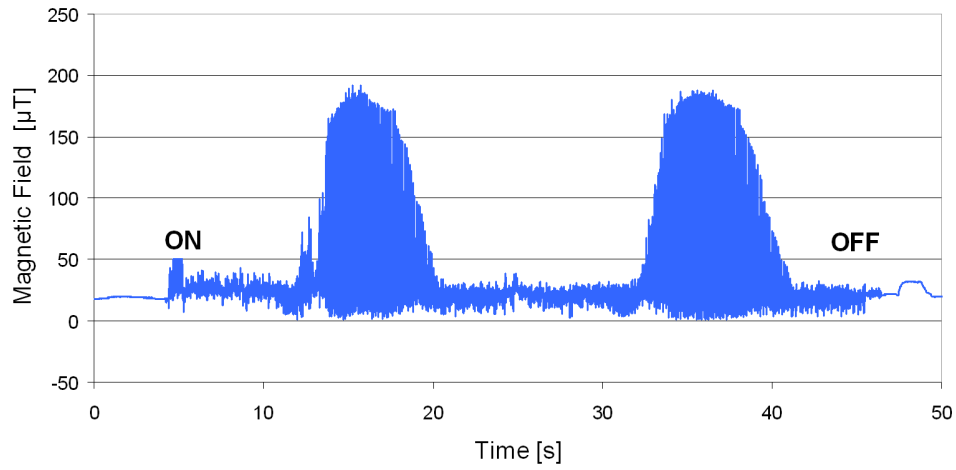


(a) Absolute value of the magnetic field

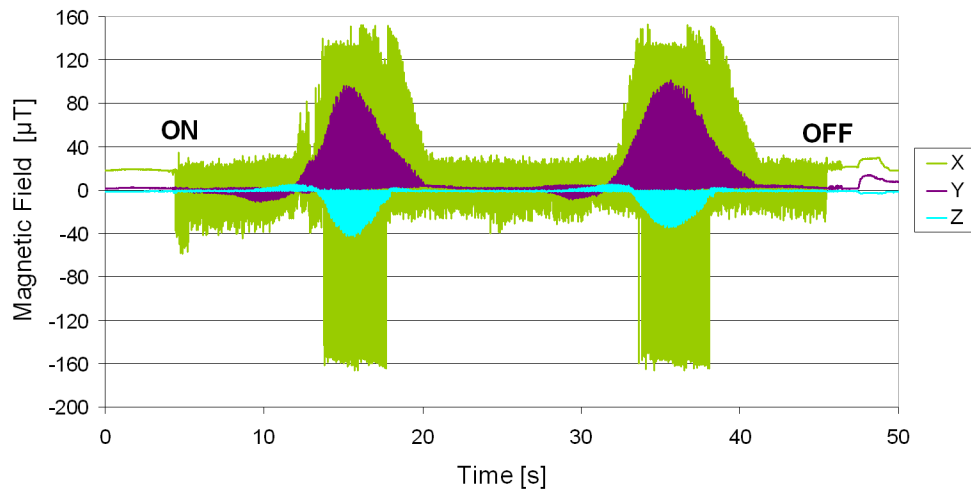


(b) Component-wise representation of the magnetic field

FIGURE 6 – Time course of the magnetic field measured at a distance of 1 cm of a filament lamp (specification in Appendix)



(a) Absolute value of the magnetic field



(b) Component-wise representation of the magnetic field

FIGURE 7 – Time course of the magnetic field measured at a distance of 1 cm of a drilling machine (body) running at constant rotational speed (specification in Appendix)

create magnetic fields that are characterised by a very fast decay behaviour with increasing distance.

For the sake of completeness, it should be mentioned that the above made assumption is not valid in particular cases, for example machines using and/or creating very strong magnetic fields, such as magnetic resonance imaging scanners, induction smelting furnaces, strong electric motors or the like. As those apparatus are usually found under special circumstances, they are not going to be the object of further investigation in this work.

TABLE 1 – Representative values of the magnetic field of domestic appliances at different distances [3]

Device	Magnetic field at a distance of 3 cm [μT]	Magnetic field at a distance of 30 cm [μT]	Magnetic field at a distance of 1 m [μT]
Hair-drier	6-2000	0.01-7	0.01-0.3
Shaver	15-1500	0.08-9	0.01-0.3
Vacuum cleaner	200-800	2-20	0.13-2
Fluorescent light	40-400	0.5-2	0.02-0.25
Microwave oven	73-200	4-8	0.25-0.6
Radio (portable)	16-56	1	≤ 0.01
Cooker	1-50	0.15-0.5	0.01-0.04
Washing machine	0.8-50	0.15-0.3	0.01-0.15
Iron	8-30	0.12-0.3	0.01-0.03
Dishwasher	3.5-20	0.6-3	0.07-0.3
Computer	0.5-30	< 0.01	≈ 0
Television (tube)	2.5-50	0.04-2	0.01-0.15

2.1.1 Complement : Magnetic Field of Rotating Iron or Steel Masses

Just as in the case of the geomagnetic field, iron and ferrous masses rotating in an already existing magnetic field induce an additional magnetic field. The so-called self-induction originates from the ferromagnetic properties of the rotating material and is related to induction currents. Interestingly, the resulting magnetic field is a function of the rotational speed. This effect can be seen in figure 8, which depicts the magnetic field at 1 cm distance to the head of a drilling machine. The number of revolutions was constantly increased until $t \approx 3$ s and then equably decreased. At $t \approx 2$ s the Nyquist frequency is reached and aliasing-effects occur. Nevertheless, the magnetic field induced by the rotation of the steel drill chuck within the Earth's magnetic field is well recognisable. A comparison between figure 8 and 6 shows that such emitters can be treated as equivalent to AC magnetic field sources and can thus be modelled by an oscillating magnetic dipole.

2.2 Cabling

Concerning cabling and electric installations, a differentiation between alternating current (AC) and three-phase current is required. For a simple AC cable measurements have shown that the magnetic field is very weak and the loss is incredibly fast with increasing distance ($1/r^2$). For example, a cable passed through with 10 A alternating current cannot be detected at 10 cm distance.

The *three conductors within an AC cable*, namely the return wire, the supply wire and the

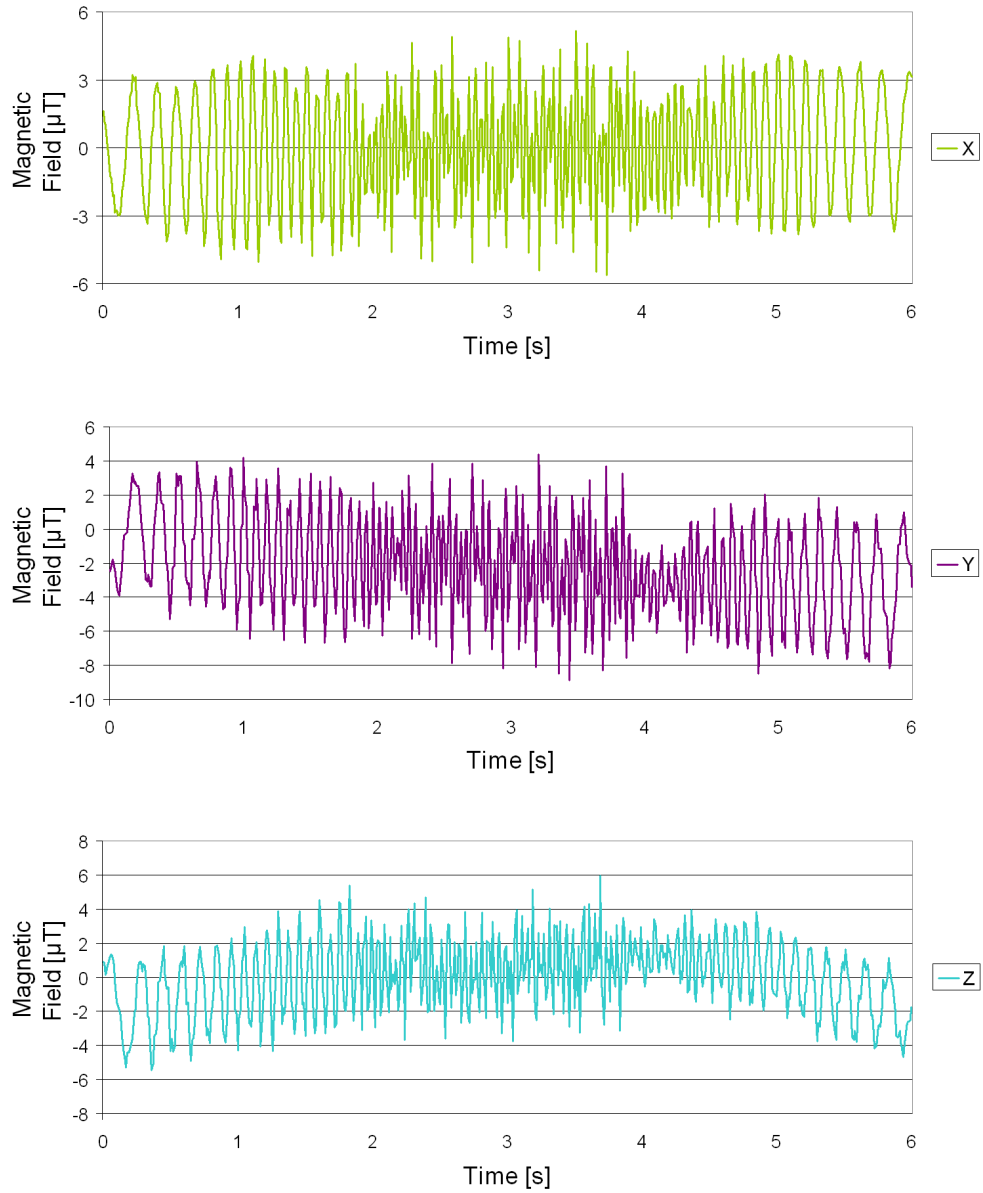


FIGURE 8 – Time course of the three components of the magnetic field measured at a distance of 1 cm of a drill chuck (hand drill), the number of revolutions is varied

grounding, can easily be approximated as current-carrying straight wires of infinite length. This means, it applies :

$$B = \mu_0 \mu_r \cdot \frac{I}{2\pi \cdot r}$$

The magnetic field decay is thus proportional to $1/r$. Moreover, the sign of the magnetic field depends on the direction of the current I , which is always of opposite sign for the supply and return conductor. Due to the closeness within the cable, their magnetic fields superimpose in an *almost obliterative manner* [19]. The grounding cable usually only transmit a current in case of a defect. Hence, the field of an AC cable as a whole is merely measurable, even though each wire itself creates a magnetic field decaying with $1/r$.

The case of two conductors at a relatively small distance and with currents in opposite direction will reappear in the following sections in this or a similar form. Therefore, it should be pointed out that the magnetic field loss is usually described by a $1/r^2$ -characteristic [1].

However, for a *three-phase current cable* the situation is not that simple. It consists of five conductors of which three carry 50 Hz alternating currents, each phase-shifted by $\pm 120^\circ$ in comparison with the other two currents. In case of a balanced load of all three phases the sum of the three currents at all points and times is zero. Due to the closeness of the conductors, the induced magnetic fields would also nearly sum up to zero.

But, *for a household supply system this is not always be the case*. For example, the three-phase current might be split into three alternating currents at a subsequent point of the power supply system; if only one of the electric consumers supplied by the alternating currents is active, this inevitably results in an unbalanced load of the three phases. As normally there is no voltage applied to the grounding cable, here the fifth wire, called the neutral conductor, comes into play. It serves as a return conductor but is only carrying a current, if the load of the three phases is unbalanced and the currents do not sum up to zero. This current through the neutral conductor is equal to that sum, but reversed in direction.³, see figure 9. Applying the same obliteration-principle as for the alternating current cable, the total magnetic field induced by a three-phase current cable is thus close to zero. Its magnetic field loss characteristic can also be described by $1/r^2$. [1]

In summary, alternating and three-phase current cables are very unlikely to affect magnetometers due to their weak magnetic fields and the fast field loss with increasing distance.

3 Public Electricity Supply

As mentioned in the preceding section, most European countries, including Germany and France, the public electric energy supply use three-phase alternating current at 50 Hz. Households and small businesses are usually supplied with 400 V. But the long-haul transmission takes place at high voltage and low current levels in order to minimise the losses, which are proportional to the intensity of the current. In the so-called transmission grid, consisting of the extra high and high voltage grid, the electric energy is transported from the source to the main consumer points. There it is either used, e.g. for rail-traffic or large scale industries, or transported to smaller consumers through the medium and low voltage grid. Together, those two form the distribution grid.

At the end of 2011 the French electricity transmission grid had an overall length of 104100 kilometres. Some 54% of these are accounted for by the high voltage grid operating at 150 kV, 90 kV and 63 kV; the remainder is allotted to the extra high power grid using 225 kV and 400 kV [17]. The medium and the low voltage grid work at 1 – 50 kV, respectively < 1 kV

3. This only applies for linear consumers, that is to say electric consumers that do not create harmonics. Harmonics can severely affect the current on the neutral wire, but are not further discussed.

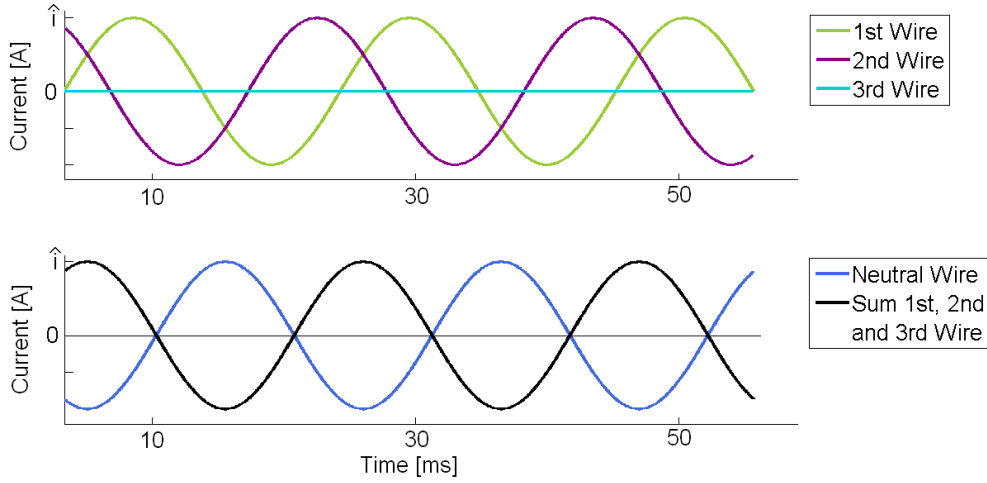


FIGURE 9 – Currents in the wires of a three-phase alternating current cable in case of an unbalanced phase load

and have an overall length of over 1.3 million kilometres [7].

Germany is equally pervaded by its electricity network : the transmission grid has a total length of 113000 kilometres, whereas the distribution grid nearly sums up to a length of 1.7 million kilometres. Unlike France, the extra high voltage grid operates at 380 and 225 kV ; the high voltage grid uses between 60 kV and 110 kV [4].

Just like every other current-carrying wire, power supply lines create magnetic fields that might be sensed. We are going to take a closer look at the different grids with a focus on the higher voltages (380, 225 and 110 kV), because they are also related to higher currents. Equivalent data for the French voltages can be found in [9]. Unfortunately, owing to the lack of detailed electricity grid maps and the (volitional) distance to inhabited areas, we were not able to carry out own measurements.

3.1 Overhead Power Lines

Due to their easy maintenance and good heat dissipation abilities, overhead power lines form the greatest part of the high and extra high voltage grid. The magnetic field created by an aerial line depends on many factors, e.g. the type of the pylons, the number of conductor ropes, the cables sag and even the weather conditions. [19] Moreover, the capacity utilisation strongly depends on the energy demand, which varies over the day and over the year. For this reason, any type of general statement can only be based on an exemplary study.

3.1.1 Spatial Course of the Magnetic Field Created by Overhead Power Lines

The most common type of transmission tower in Germany is the *Donau* pylon, a two-level pylon with 6 hang-points, each equipped with $n_w \in \{1, 2, 4\}$ wires depending on the voltage. This means, such a tower is able to transmit $2 \cdot n_w \times$ three-phase current. [13] The geometric dimensions of a *Donau* pylon are shown in figure 10. It is very suitable to serve as an example because it resembles the *Beaubourg* pylon, which is mostly used in France.

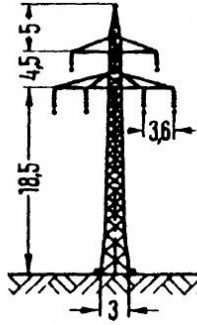


FIGURE 10 – Geometric dimensions of a *Donau* pylon [13]

Figure 11 shows the spatial course of the root mean square value of the magnetic field underneath an overhead power line with *Donau* pylons. It is based on Copperfield® calculations, a software particularly designed to compute electromagnetic fields. The following conditions and assumptions were defined [19] :

1. The distance to the ground is always 1 m.
2. The pylons are in the zero position.
3. The distance of the conductor ropes from the earth is assumed to be 12 m at the position of maximal cable sag.
4. The distance (abscissa) is increased crosswise to the power line's route at the point of maximum cable sag and parallel to the ground.
5. The voltages stated in the legend of figure 11 are only nominal values, meaning that the actual voltages could differ. As in reality the operating voltages are usually higher than the nominal ones, they were chosen as follows for the calculation : $u_{real}(380 \text{ kV}) = 430 \text{ kV}$, $u_{real}(220 \text{ kV}) = 245 \text{ kV}$, and $u_{real}(110 \text{ kV}) = 123 \text{ kV}$.
6. The power line runs at full capacity utilisation. It follows that the current in each wire is the maximum operating current dependant on the voltage : $\hat{i}(380 \text{ kV}) = 2.58 \text{ kA}$, $\hat{i}(220 \text{ kV}) = 1.29 \text{ kA}$ and $\hat{i}(110 \text{ kV}) = 0.535 \text{ kA}$.
7. The number of wires installed at each hang point is generally : $n_w(380 \text{ kV}) = 4$, $n_w(220 \text{ kV}) = 2$ and $n_w(110 \text{ kV}) = 1$. [13] As these n_w wires are very close to each other and moreover carrying currents with the same phase shift, they are considered as one wire passed through with $n_w \cdot \hat{i}$.
8. There are interactions with other power lines.

Figure 11 indicates that magnetic fields created by aerial power lines could be detected by magnetometers, in case they are close enough. As one might expect, the power lines working at higher intensities of current are also the source of stronger magnetic fields.

But, what about the variation over time apart from the daily variation? If the conductors carrying the three phases were very close to each other, the resulting magnetic field would be nearly zero. This is not the case : Figure 10 shows that their distances are 3.6 and 4.8 m. Hence, the magnetic field that can be measured at fixed distance to the power line results from the superimposition of several magnetic fields ; all alternating at a frequency of 50 Hz, but with different phase shifts and amplitudes.

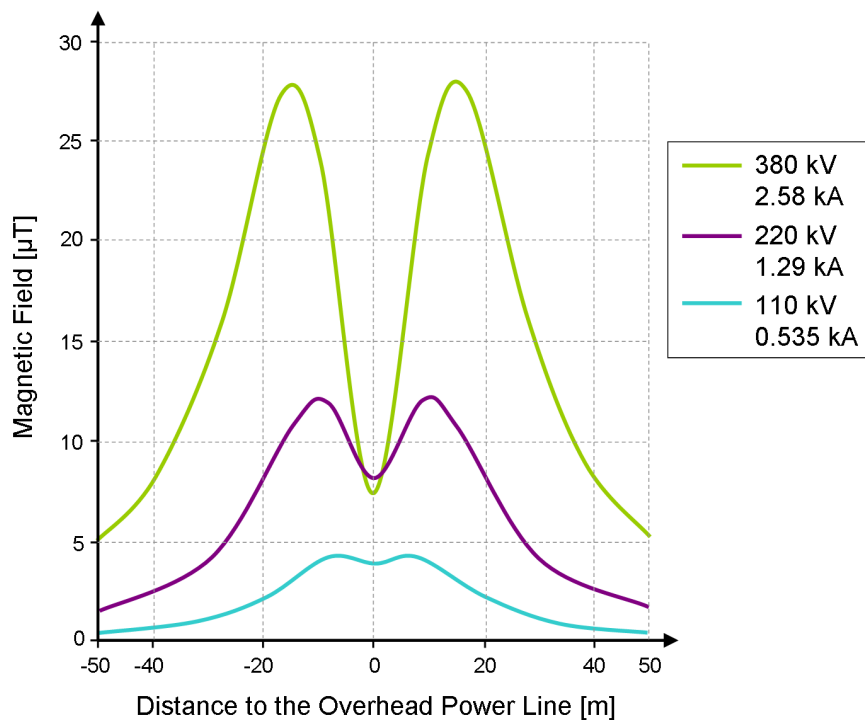


FIGURE 11 – Calculated spatial course of the magnetic field (RMS) underneath an overhead power line at 1 m distance to the ground and crosswise to the power line’s route at the point of maximal cable sag [19]

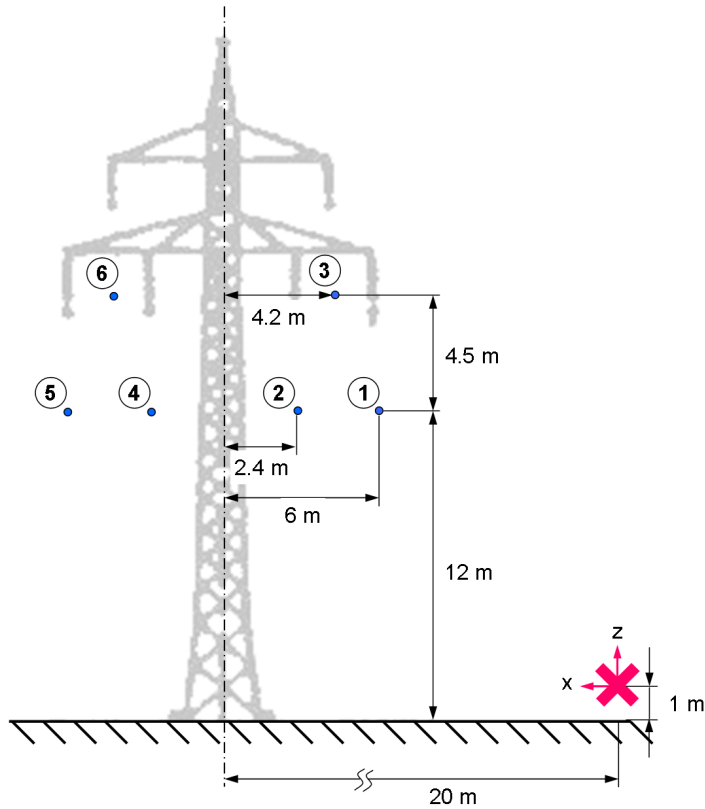


FIGURE 12 – Schematic sectional drawing of an overhead power line at the point of maximal cable sag with specification of the geometric dimensions

3.1.2 Time Course of the Magnetic Field Created by an 380 kV Overhead Power Line

To get an idea of the superimposition of the magnetic fields created by the conductor ropes of an overhead line, we will exemplarily study the magnetic field of the 380 V (nominal voltage) aerial line under the same conditions as in the preceding example. So here as well, we have $n_w(380\text{kV}) = 4$, $\hat{i}(380\text{ kV}) = +2.58\text{ kA}$ passing through each individual wire and $f = 50\text{ Hz}$. Moreover, the 4 wires at each hang-point are again considered as one conductor carrying the sum of the four operating currents, see figure 12. The distance to the point of maximal cable sag is fixed at +20 m. The resulting defined point $P = (0,0)$, which is the origin of the used coordinate system, is marked with a red cross in figure 12.

With c being the speed of light and

$$(1) \quad \varphi(x, z) = \arctan\left(\frac{x}{z}\right)$$

$$(2) \quad \mathbf{e}(x, z) = \begin{pmatrix} -\cos(\varphi(x, z)) \\ \sin(\varphi(x, z)) \end{pmatrix}$$

$$(3) \quad r(x, z) = \sqrt{x^2 + z^2}$$

TABLE 2 – Parameters for the calculation of figure 13

Wire	\mathbf{x} [m]	\mathbf{z} [m]	\mathbf{r} [m]	φ [rad]	Phase $\Delta\varphi$ [rad]
1	14	11	17.8	0.90	$2\pi/3$
2	17.6	11	20.75	1.01	0
3	15.8	15.5	22.13	0.79	$4\pi/3$
4	22.4	11	24.95	1.11	0
5	26	11	28.23	1.17	$2\pi/3$
6	24.2	15.5	28.74	1.00	$4\pi/3$

we can approximate the x - and z -component of the vector of the magnetic field in P by :

$$(4) \quad \begin{pmatrix} B_x(t) \\ B_z(t) \end{pmatrix} = \sum_{j=1}^6 \mathbf{B}_{w,j}(t)$$

$$(5) \quad = \frac{\hat{i}}{3} \cdot \frac{\mu_0 \cdot \mu_{r,air}}{2\pi} \cdot \sum_{j=1}^6 \left[\frac{\mathbf{e}(x_j, z_j)}{r(x_j, z_j)} \cdot \sin \left(2\pi f \cdot \left(t - \frac{r(x_j, z_j)}{c} \right) + \Delta\varphi_j \right) \right]$$

The y -component is not affected as the y -axis is assumed to be parallel to the conductors. Moreover, equation 5 implies the approximation of the cables as straight conductors of infinite length.

These sure are severe simplifications of the real problem. But nonetheless it allows us to get a rough estimate of the expected time course of the magnetic field, as shown in figure 13. The three graphs are based on table 2, which in turn results from the geometric properties of the problem, given in figure 12. The time scale is chosen to be small in order to properly display the oscillations. It is important to point out that the measured time course by a magnetometer would look different due to the low sample frequency of 100 Hz.

With this set of parameters, the x -component of the magnetic field vector varies between $\pm 31.32 \mu\text{T}$, whereas the z -component alternates between $\pm 13.33 \mu\text{T}$. Resulting from a superposition of several phase-shifted 50 Hz sine-waves, the sinusoidal form and the frequency remain unchanged. But even when the distance to the overhead power line is dramatically increased to 50 m, the fluctuations can still be detected by magnetometers. The same applies for a current reduction to $\hat{i} = 1.29 \text{ kA}$ (corresponding to 220 kV), but no longer for $\hat{i} = 0.535 \text{ kA}$ (corresponding to 110 kV).

However, in vicinity of high voltage overhead power lines the basic requirement of a stationary magnetic field is thus no longer fulfilled.

3.2 Underground Cables

Underground cables are mostly installed in the medium and low voltage grid, but also in the high voltage grid up to 110 kV. Such cables consist of three conductors carrying 50 Hz alternating currents, each phase-shifted by $\pm 120^\circ$ as usual for three-phase current. The difference to the cables discussed in section 2 lies in the fact that there is no ground and no neutral wire. Moreover, the three conductors have a greater distance for reasons of

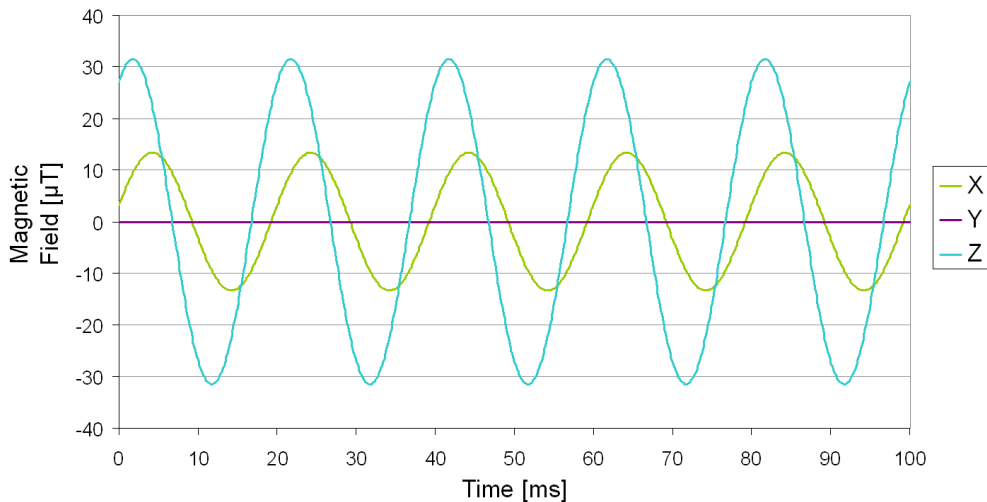


FIGURE 13 – Calculated time course of the three components of the magnetic field at 20 m distance to an 380 V overhead power line

heat dissipation. The magnetic field in the surrounding of such underground cables is to be exemplary examined for 110 V.

3.2.1 Spatial Course of the Magnetic Field Created by an 110 kV Underground Cable

Figure 15 shows the spacial course of the root mean square value of the magnetic field⁴ of an 110 V underground cable. The following conditions and assumptions were set [19] :

1. The distance to the ground is always 1 m.
2. The underground cable is in the $x = 0$ m, $z = -2.2$ m position (figure 14).
3. The distance (abscissa) is increased crosswise to the direction of the underground cable and parallel to the ground.
4. The cross-sectional area of each conductor is 630 mm^2 .
5. The strength of the current of each phase is $\hat{i} = 0.64 \text{ kA}$; the phase load is balanced.
6. There are no interactions with other underground cables.

As can be see from figure 3.2 the magnetic field induced by an 110 kV underground cable can only be distinguished from the measurement noise ($1.35 \mu\text{T}$) at $|x| < 3$, which is equivalent to a distance of 3.72 m. This value will be lower for underground cables installed in the medium and low voltage grid.

3.2.2 Time Course of the Magnetic Field Created by an 110 kV Underground Cable

However, keeping in mind that the wires of the cable are passed through with phase shifted alternating current, the induced magnetic field is subject to fluctuations over time.

4. calculated with Copperfield®

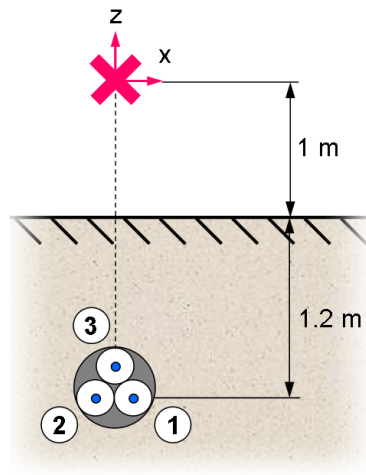


FIGURE 14 – Schematic sectional drawing of an underground cable with specification of the relevant geometric dimensions

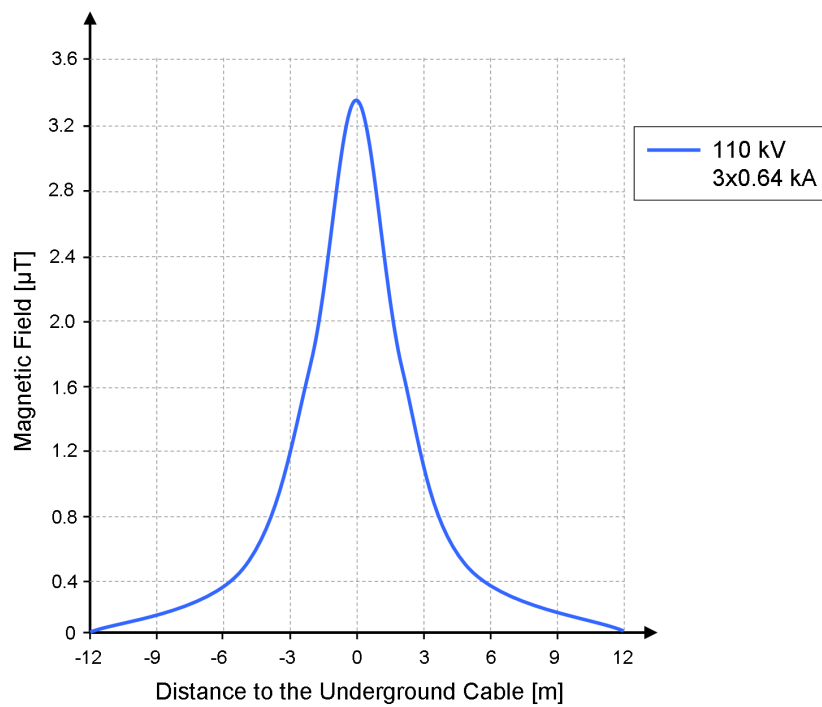


FIGURE 15 – Calculated spacial course of the magnetic field (RMS) above an 110 V underground cable at 1 m distance to the ground and crosswise to the direction of the cable [19]

TABLE 3 – Parameters for the calculation of figure 16

Wire	\mathbf{x} [m]	\mathbf{z} [m]	\mathbf{r} [m]	φ [rad]	Phase $\Delta\varphi$ [rad]
1	0	2.157	2.157	0	$2\pi/3$
2	0.025	2.2	2.2	0.011	0
3	-0.025	2.2	2.2	-0.011	$4\pi/3$

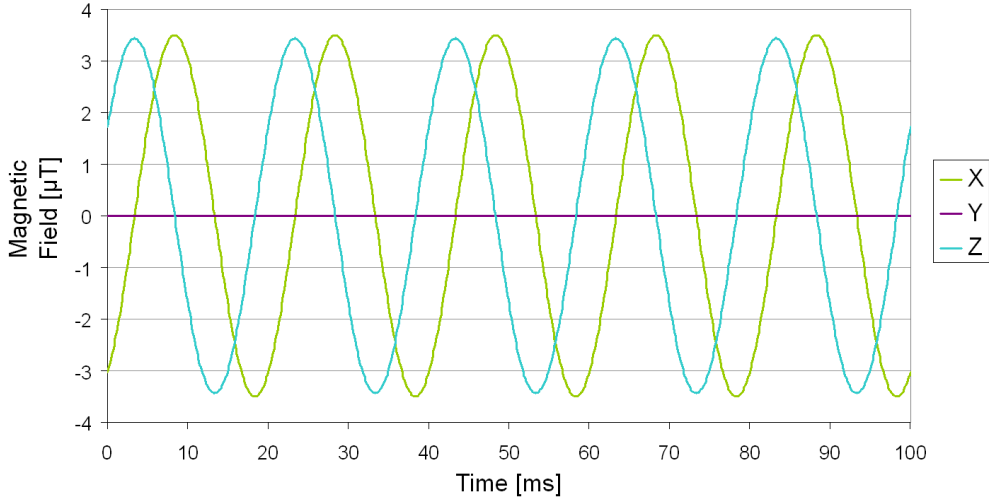


FIGURE 16 – Calculated time course of the three components of the magnetic field at 2.2 m distance above an 110 V underground cable

Using equation 1, 2 and 3, the magnetic field can be calculated similar to the overhead power line by :

$$(6) \quad \begin{pmatrix} B_x(t) \\ B_z(t) \end{pmatrix} = \sum_{j=1}^3 \mathbf{B}_{w,j}(t)$$

$$(7) \quad = \frac{\hat{i}}{3} \cdot \frac{\mu_0 \cdot \mu_{r,air}}{2\pi} \cdot \sum_{j=1}^3 \left[\frac{\mathbf{e}(x_j, z_j)}{r(x_j, z_j)} \cdot \sin \left(2\pi f \cdot \left(t - \frac{r(x_j, z_j)}{c} \right) + \Delta\varphi_j \right) \right]$$

Inserting the values listed in table 3, figure 16 is obtained. The similarity to figure 13 is obvious. But, the x -component of the magnetic field vector only varies between $\pm 3.42 \mu\text{T}$, whereas the z -component alternates between $\pm 3.48 \mu\text{T}$.

3.3 Transformation stations

Transformation stations, which also form a key part of the public electricity supply system, are to be mentioned in the context for the sake of completeness. All available sources, e.g. [9] and [19], state that the magnetic fields induced by transformation stations are weak

compared to those of underground cables and overhead lines. Also the field decreases very rapidly with increasing distance to the station.

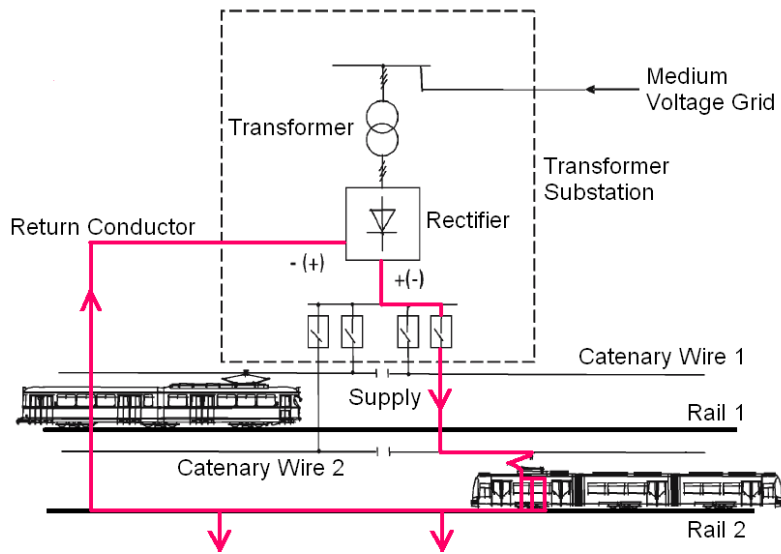


FIGURE 17 – Principle structure and functional principle of the power supply of a direct current railway system [8]

4 Electricity Supply of Public Transport Systems

For the investigation of low-frequency magnetic fields intercity and inner-city public rail transport systems are of a great importance. In particular, it is the carefully thought-out energy supply system that is of interest.

Due to economical and historical reasons, many different types of railway systems and traction power systems have emerged, which differ from country to country and also from city to city. The voltages vary between 600 V to 50 kV, the frequencies range from 0 Hz, that is to say direct current, to 60 Hz alternating current. However, the general principle of the power supply, presented in figure 17, is always similar : the trains are permanently connected to one or several current-carrying conductors, usually overhead wires or a third rail, by a pantograph or a collector. The rails function as return conductors and are partly earthed to avoid dangerously high voltages. Both, return and supply conductors end in a transformer substation, which in turn is supplied by the medium voltage grid in most cases. The transformer substations are placed alongside the rail in distances that vary from several, up to 100 km. The contact line, the engine, the rails and the transformer substation thus form an enormous electric circuit. Further details can be found in [8] or [19].

From the rail power supply, regardless of whether for trains, metros or tramways, arise several possible problems. First, the conductors are passed through by more or less strong currents (> 100 A); for example the later discussed RER trains require 413 A at 50% motor load. As the distances of the return and supply conductors are not negligible, their magnetic fields do not cancel each other.

Secondly, the rails are partly earthed. This means that the *return current level is markedly lower than the supply current level*, meaning their magnetic fields differ significantly strength. As both currents are of opposite direction, the magnetic field induced by the catenaries or the third rail is less compensated as in a fictive non-earthed case.

Thirdly and lastly, the magnetic fields only appear, if the respective section of the route is

being passed through by a train. In consequence, the time course is difficult to predict and impossible to be described by an analytical function. Moreover - and that is an even greater problem - the magnetic field created by highly-frequented railway systems with short supply segments ($< 5 \text{ km}$), tends to fluctuate vastly in very short time-scales. This applies for the Parisian innercity train system depicted in figure 18.

Due to the extreme variety of systems, it is impossible to examine all different kinds of cases. Just like for the public electricity supply systems, we will try to gain generally valid statements from a thoroughly chosen example. As the magnetic field of straight conductors at alternating current was already studied for the overhead power line and the underground cable, we are going to examine a direct current railway system, more precisely the Parisian suburban train. Inter-city trains, which are usually working with AC current, are shortly discussed.

4.1 Direct Current Railway Systems

The RER, which stands for *Réseau Express Régional*⁵, is the suburban train of Paris. It connects the inner-city district of Paris with its suburbs and airports through a traffic network composed of 5 lines (A-E) and over 240 stations.

Outside of Paris the RER is operated by the SNCF (*Société Nationale des Chemins de Fer Français*)⁶, the national railway company running most of the French rail services. This part uses 25kV/50 Hz alternating current, just as regular and express trains in France. But, because the network was established in the late 1960ths and early 70ths, neither major changes of the urban energy supply infrastructure nor of the subterranean railroad system were possible. For this reason, within the city the RER uses mostly the Parisian metro network and the appending power supply system providing 750 V *direct current*. In this area it is operated by the RATP (*Régie Autonome des Transports Parisiens*)⁷, which is responsible for the majority of the local public transport systems of Paris including the metro. Consequently, the trains serving the RER network have the extraordinary characteristic of being able to run with both direct and alternating current without stopping.

In order to demonstrate the magnetic impact of a public transport system, we will take a closer look at the RER B. This line runs from *Charle de Gaulle Airport/Mitry-Clay* to *Robinson/Saint-Rémy-lès-Chevreuse* and creates a 80 km North-South link. It serves, among others, the station *Luxembourg*, located less than a one minute walk from the *Centre Automatique et Systèmes* (CAS) at 60, Boulevard Saint-Michel in central Paris.

The section between the stations *Luxembourg* and *Cité Universitaire* (see figure 18) is particularly suited to serve as an example. First and foremost, it is close to the *Ecole Supérieure des Mines de Paris*, which substantially facilitates the execution of measurements. Secondly, all the stations in the section are exclusively served by the RER B and no further RER or metro lines. This has the advantage that the traffic can be traced easily and only two directions need to be considered. Moreover, the number of trains travelling in the section and thus inducing a magnetic field can be estimated from the schedule with ease.

Thirdly and lastly, the tracks between the corresponding electrical substations *Montsouris* and *Luxembourg* form a relatively straight section of the route, as can be seen from figure 18. This enables modeling the catenaries and the rails as straight conductors of infinite length for the calculations.

5. Regional Express Network

6. French National Railway Corporation

7. Autonomous Operator of Parisian Transports

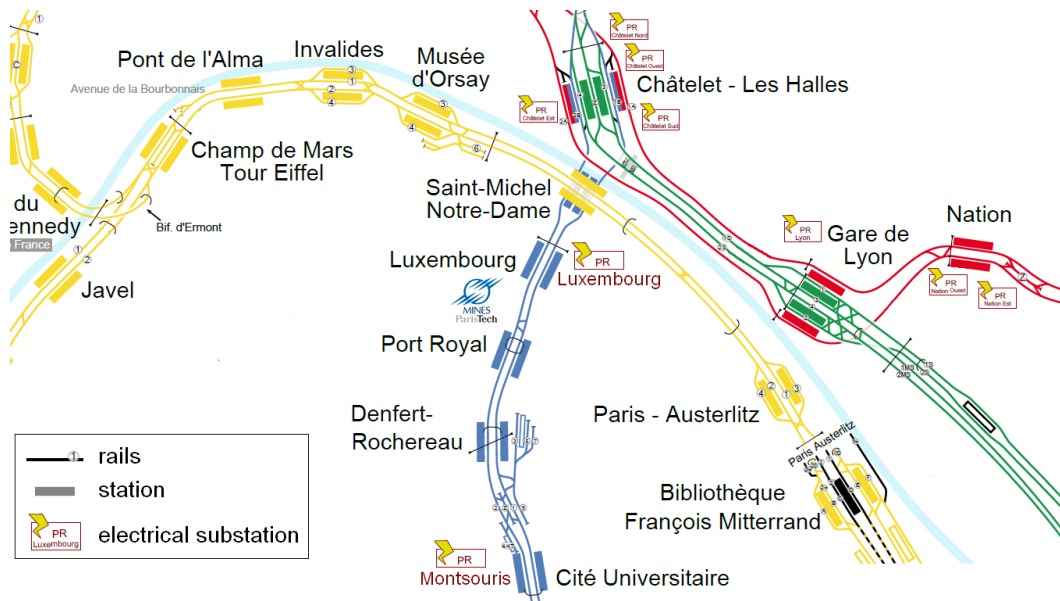


FIGURE 18 – Detail of the RER railway map around the station *Luxembourg* [11]

4.1.1 Measurement of the Magnetic Field Created by the RER B

Figure 19 shows the three components of the magnetic field measured at approximately 24 m distance to the RER B line over the course of 10 hours. The measurements were conducted inside the *Centre Automatique et Systèmes* (CAS); for further dimensional details see figure 20. The axes of the sensor were oriented as such that the x -axis points northwards, the y -axis points eastwards and the z -axis points into the ground. At first sight, the chosen time scale might seem unusual. But, the interest of this measurements was to show that the major part of the disturbances, measurable in the CAS during the day, can be traced back to the RER that is not running during night.

What stands out immediately, is the lack of disturbances - apart from the measurement noise - between 1 :30 and 4 :50 am. Reasonably assuming that the last train according to the timetable is not necessarily the "real" last train, such as cleaning or repair trains, figure 19 matches the RER timetable. The last official train leaves the section at exactly 1 :00 am, whereas the first official train enters at 5 :18 am [16]. This hypothesis is supported by the fact that the fluctuations decrease smoothly before reaching the constant level of measurement noise. As the number of trains is reduced during low-traffic periods, this also matches the RER timetable [16]. Furthermore figure 19 indicates that the fluctuations of the magnetic field during the day are strong : the x -component varies between $17.96 \mu\text{T}$ and $8.88 \mu\text{T}$, the y -component between $8.29 \mu\text{T}$ and $-4.57 \mu\text{T}$ and the z -component alternates between $44.24 \mu\text{T}$ and $27.42 \mu\text{T}$.

In conclusion, one probable hypothesis can be derived from figure 19, which will be differently approached in the following section. The RER creates a strong fluctuating magnetic field that is measurable at large distances and clearly surpasses the detection level of $1.35 \mu\text{T}$ of the common magnetometers. In consequence, this would mean that all measurements conducted in the CAS are inevitably influenced by the RER.

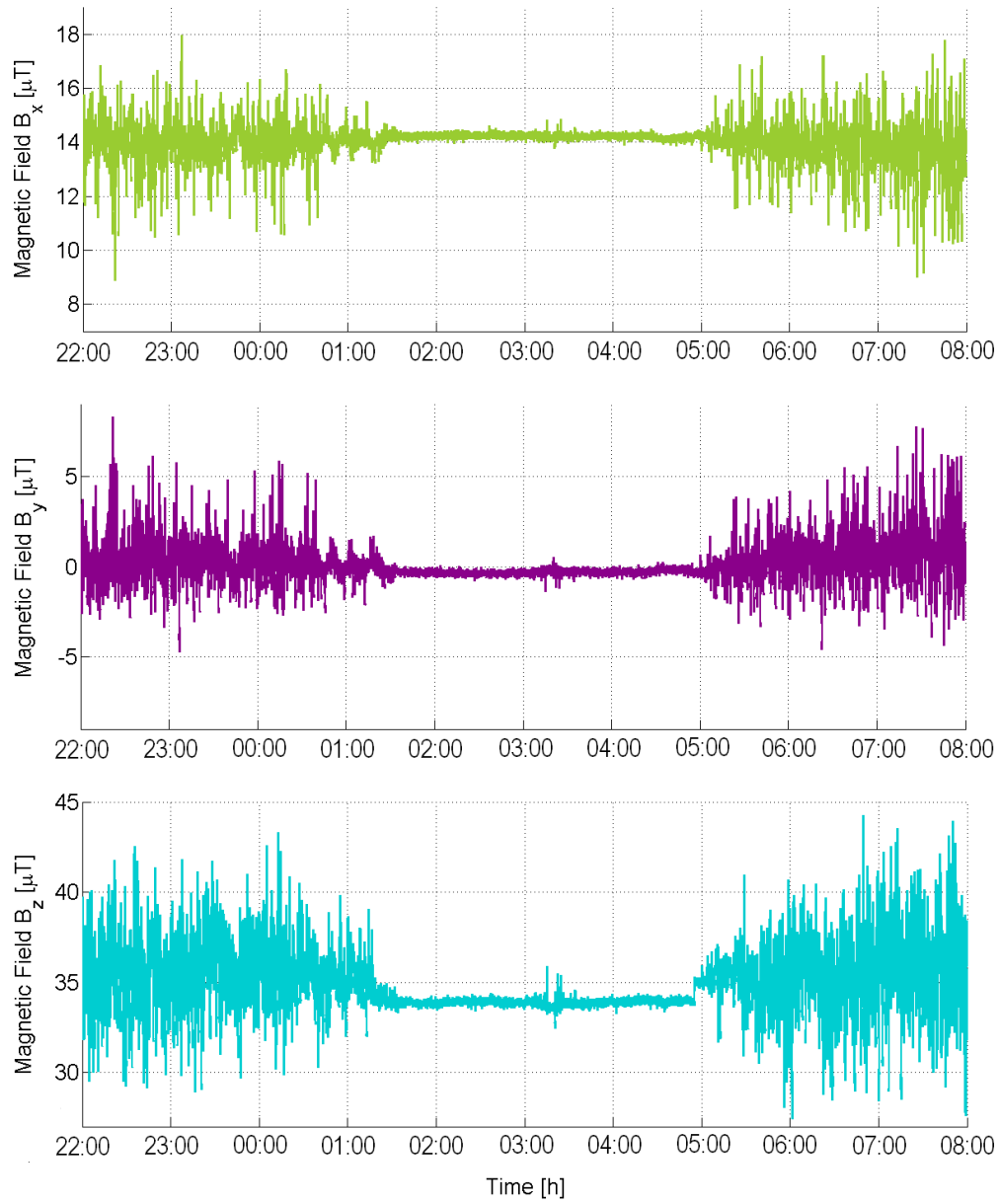


FIGURE 19 – Magnetic field created by the RER B over the course of 10 hours, measured in the CAS

4.1.2 Calculation of the Magnetic Field Created by the RER

For the subsequent calculation of the magnetic field induced in RER section between *Luxembourg* and *Cité Universitaire* (see figure 18), several assumptions and simplifications are necessary. As evidenced by the later part of this discussion, the results nevertheless give a good approximation of the measured values.

1. The trains designed for the RER B, specified as Z8100-MI79, are equipped with an engine with a rated performance of $P = 2480kW$ ⁸ at $U = 1,5kV$ direct current [15]. The 1.5 kV direct current are delivered by two catenaries, each supplied with 750 V by two electrical substations, in the studied case *PR Luxembourg* and *PR Montsouris*. Let us assume that both substations are equally charged.

$$C = 50\%$$

In other words, the engine is supplied by two equal current sources connected in parallel.

2. Reasonably, the trains do not constantly work at maximum motor load, which is only required in cases of quick acceleration or braking. The minimum, average and the maximum motor load (averaged over all the trains travelling in the section) are considered as :

$$\begin{aligned} L_{min} &= 30\% \\ L_{avg} &= 50\% \\ L_{max} &= 70\% \end{aligned}$$

3. The travel time between *Luxembourg* and *Cité Universitaire* is approximately 6 minutes. At peak traffic periods during the week⁹ the trains travel at a distance of 3 minutes, whereas at average traffic periods¹⁰ the stations are used every 3 – 6 minutes [16]. Accordingly, there are about $1 \leq n_t \leq 2$ trains driving in each direction within the considered section of line.
4. This leads to an absolute current of

$$\begin{aligned} I_{cat,1} &= n_{t,dir1} \cdot L_{dir,1} \cdot C \cdot \frac{P}{U} \\ I_{cat,2} &= n_{t,dir2} \cdot L_{dir,2} \cdot C \cdot \frac{P}{U} \end{aligned}$$

in the overhead wires. The current changes of sign depending on the direction the train is travelling in; the assignment of the signs is shown in figure 20. The current of the rails always runs in the opposite direction than the current in the corresponding catenaries.

5. As mentioned above, the catenaries and the rails are assumed to be straight conductors of infinite length. The magnetic field in their surrounding is thus described by :

$$(8) \quad B = \mu_0 \cdot \mu_r \frac{I}{2\pi \cdot r}$$

As the distance of the two overhead wires of one direction is small and both have the same direction of current, they are simply considered as one.

8. Power the electric locomotive can deliver for one hour without any danger.

9. from 7.00 to 9.30 am and 4.30 to 8.00 pm

10. from 9.30 am to 16.30 pm and after 8.00 pm

6. The rails are partly earthed to avoid high difference voltage between the rails and the soil. The non-earthed percentage, hereinafter referred to as NEA , is assumed to be :

$$NEA = 20\%$$

Each rail is supposed to carry the same current, thus 10 % of the current through the corresponding overhead wire.

All those values are subject to constant fluctuations, e.g. depending on acceleration, braking and velocity of the trains in the section. As the behavior is unpredictable, it is only possible to calculate with such estimated values. However, the assumptions and conditions previously listed, allow a simplified calculation of the magnetic field created by the RER B in the section between *Luxembourg* and *Cité Universitaire*. If the rails and overhead wires are assumed to run in y -axis direction (see figure 20), the induced magnetic field only has an x - and z -component. It is the sum of the magnetic fields of both directions, each in turn consisting of the catenaries and the rails :

$$\begin{aligned} \begin{pmatrix} B_x(t) \\ B_z(t) \end{pmatrix} &= \mathbf{B}_{dir,1}(t) + \mathbf{B}_{dir,2}(t) \\ &= [\mathbf{B}_{cat,1}(t) + \mathbf{B}_{rail,1.1}(t) + \mathbf{B}_{rail,1.2}(t)] + [\mathbf{B}_{cat,2}(t) + \mathbf{B}_{rail,2.1}(t) + \mathbf{B}_{rail,2.2}(t)] \end{aligned}$$

Taking into account equation 8 and the indices specified in table 4, we obtain the magnetic field in the origin of the right-handed coordinate system - marked with a red cross in figure 20 - by :

$$\begin{aligned} \begin{pmatrix} B_x(t) \\ B_z(t) \end{pmatrix} &= \mu_0 \cdot \mu_r \cdot \frac{I_{cat,1}(t)}{2\pi} \cdot \left[\frac{\mathbf{e}(x_1, y_1)}{r_1} - NEA \cdot \left\{ \frac{\mathbf{e}(x_2, y_2)}{r_2} + \frac{\mathbf{e}(x_3, y_3)}{r_3} \right\} \right] \\ &\quad - \mu_0 \cdot \mu_r \cdot \frac{I_{cat,2}(t)}{2\pi} \cdot \left[\frac{\mathbf{e}(x_4, y_4)}{r_4} - NEA \cdot \left\{ \frac{\mathbf{e}(x_5, y_5)}{r_5} + \frac{\mathbf{e}(x_6, y_6)}{r_6} \right\} \right] \\ (9) \quad &= \mu_0 \cdot \mu_r \cdot \frac{C \cdot P}{2\pi \cdot U} \cdot n_{t,dir1}(t) \cdot L_{dir1}(t) \cdot \left[\frac{\mathbf{e}(x_1, y_1)}{r_1} - NEA \cdot \left\{ \frac{\mathbf{e}(x_2, y_2)}{r_2} + \frac{\mathbf{e}(x_3, y_3)}{r_3} \right\} \right] \\ &\quad - \mu_0 \cdot \mu_r \cdot \frac{C \cdot P}{2\pi \cdot U} \cdot n_{t,dir2}(t) \cdot L_{dir2}(t) \cdot \left[\frac{\mathbf{e}(x_4, y_4)}{r_4} - NEA \cdot \left\{ \frac{\mathbf{e}(x_5, y_5)}{r_5} + \frac{\mathbf{e}(x_6, y_6)}{r_6} \right\} \right] \end{aligned}$$

where φ , \mathbf{e} and r are :

$$(10) \quad \varphi(x, z) = \arctan\left(\frac{x}{z}\right)$$

$$(11) \quad \mathbf{e}(x, z) = \begin{pmatrix} -\cos(\varphi(x, z)) \\ \sin(\varphi(x, z)) \end{pmatrix}$$

$$(12) \quad r(x, z) = \sqrt{x^2 + z^2}$$

The underlying principle is sketched in figure 21. Using the geometric specifications indicated in figure 20, these variables take the values listed in table 4. As the RER is supplied with direct current, the magnetic field is only time-dependant for two reasons : First, the number of trains travelling within the supply section varies for both directions. Secondly, the averaged motor load of the trains is not constant. This is represented by $n_{t,dir1}(t)$, $n_{t,dir2}(t)$ and $L_{dir1}(t)$, $L_{dir2}(t)$, even though they are not analytical functions.

As the line occupancy and the load of the trains strongly influence the results, many different combinations were tested and are shown in table 5. For the line occupancy applies :

$$(13) \quad n_{t,dir1}, n_{t,dir2} \in \{1, 2\}$$

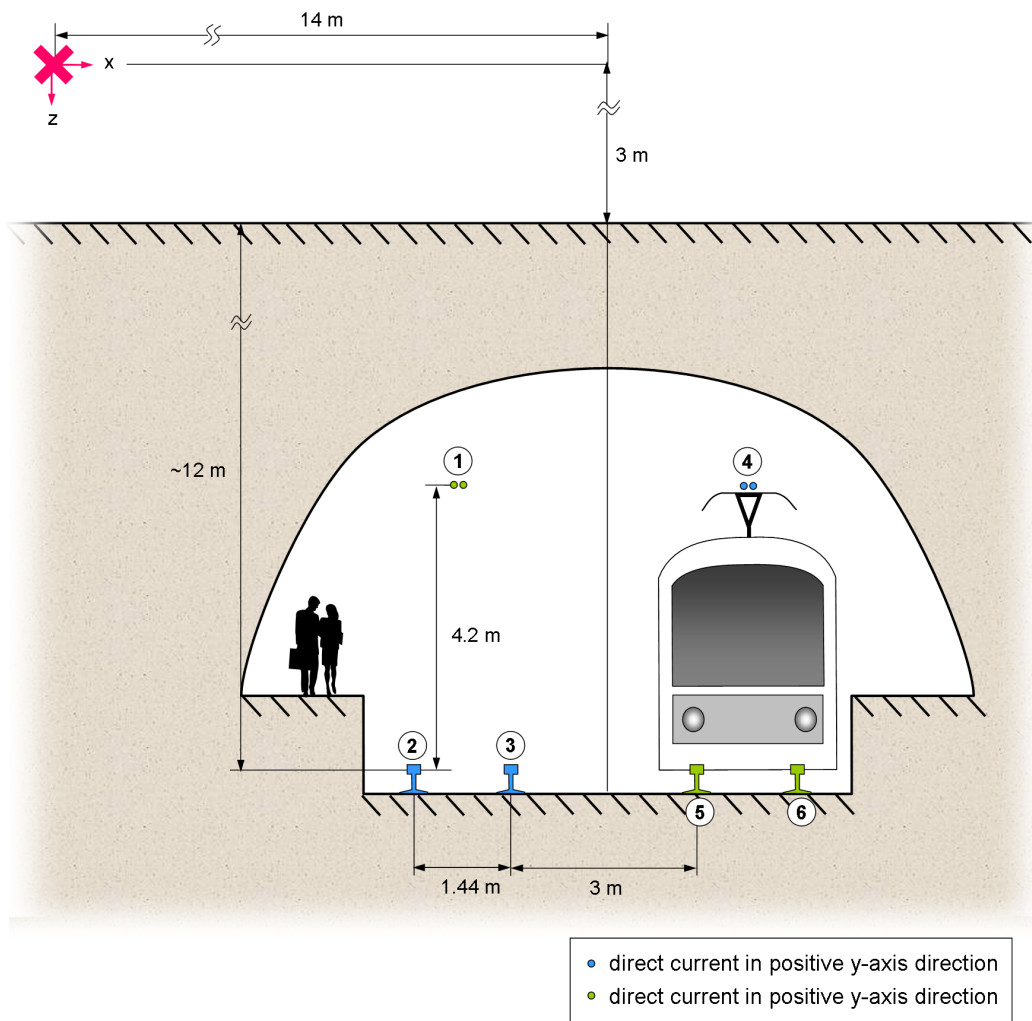


FIGURE 20 – Schematic sectional drawing of the underground RER station *Luxembourg* with specification of the geometric dimensions (from [6])

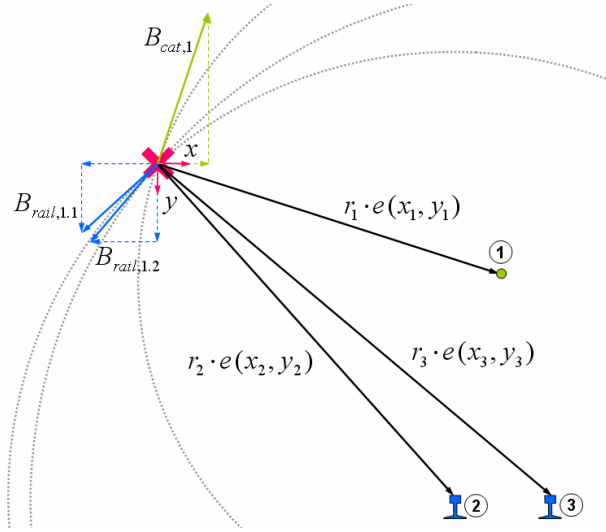


FIGURE 21 – Vector addition of the magnetic fields created by an RER rail system

TABLE 4 – Parameters for the calculation of equation 9

Wire	Index	x [m]	z [m]	r [m]	φ [rad]	I_{max} [A]	I_{min} [A]
Catenary 1	1	11.78	10.8	15.98	0.83	-248	-1157
Rail 1.1	2	11.06	15	18.64	0.64	24.8	115.7
Rail 1.2	3	12.5	15	19.53	0.69	24.8	115.7
Catenary 2	4	16.22	10.8	19.49	0.98	248	1157
Rail 2.1	5	15.5	15	21.57	0.8	-24.8	-115.7
Rail 2.2	6	16.94	15	22.63	0.85	-24.8	-115.7

whereas the motor load is :

$$L_{dir,1}, L_{dir,2} \in \{L_{min}, L_{avg}, L_{max}\}$$

More precisely, table 5 displays the calculated values of the x - and z -component of the magnetic field in the observed point P depending on the respective conditions. The x -component varies between $-3.47 \mu\text{T}$ and $6.77 \mu\text{T}$; the z -component fluctuates between $-7.39 \mu\text{T}$ and $6.38 \mu\text{T}$. These extremes result from situations, when the currents in both directions greatly differ, e.g. *when there are many trains at high motor load driving in one direction while there is only one train at low motor load travelling in the other direction*. But, both x - and z -component can also take all intermediate values.

In a completely theoretical view, we can deduce from table 5 that especially variations in the line occupancy and in the velocity profiles of the trains result in rapid changes of the induced magnetic field. These changes occur in all different kinds of situations : a train leaves the section, a train enters the section, a train breaks while arriving in a station, a train accelerates while leaving a station, etc.

TABLE 5 – Calculated values of the x - and z -component (according to model (4.18)) of the magnetic field created by the RER B for different motor loads and line occupancies

	$n_{t,dir1}$	1	1	2	2
	$n_{t,dir1}$	1	2	1	2
$load_{dir1}$	$load_{dir2}$				
30 %	30 %	$B_x = 0.58 \mu\text{T}$ $B_z = -0.18 \mu\text{T}$	$B_x = -0.52 \mu\text{T}$ $B_z = 1.61 \mu\text{T}$	$B_x = 2.27 \mu\text{T}$ $B_z = -2.14 \mu\text{T}$	$B_x = 1.17 \mu\text{T}$ $B_z = -0.36 \mu\text{T}$
30 %	50 %	$B_x = -0.15 \mu\text{T}$ $B_z = 1.02 \mu\text{T}$	$B_x = -2.00 \mu\text{T}$ $B_z = 4.00 \mu\text{T}$	$B_x = 1.53 \mu\text{T}$ $B_z = -0.95 \mu\text{T}$	$B_x = -0.31 \mu\text{T}$ $B_z = 2.03 \mu\text{T}$
30 %	70 %	$B_x = -0.89 \mu\text{T}$ $B_z = 2.21 \mu\text{T}$	$B_x = -3.47 \mu\text{T}$ $B_z = 6.38 \mu\text{T}$	$B_x = 0.80 \mu\text{T}$ $B_z = 0.24 \mu\text{T}$	$B_x = -1.78 \mu\text{T}$ $B_z = 4.42 \mu\text{T}$
50 %	30 %	$B_x = 1.71 \mu\text{T}$ $B_z = -1.49 \mu\text{T}$	$B_x = 0.60 \mu\text{T}$ $B_z = 0.30 \mu\text{T}$	$B_x = 4.52 \mu\text{T}$ $B_z = -4.77 \mu\text{T}$	$B_x = 3.42 \mu\text{T}$ $B_z = -2.98 \mu\text{T}$
50 %	50 %	$B_x = 0.97 \mu\text{T}$ $B_z = -0.30 \mu\text{T}$	$B_x = -0.87 \mu\text{T}$ $B_z = 2.69 \mu\text{T}$	$B_x = 3.78 \mu\text{T}$ $B_z = -3.57 \mu\text{T}$	$B_x = 1.94 \mu\text{T}$ $B_z = -0.59 \mu\text{T}$
50 %	70 %	$B_x = 0.23 \mu\text{T}$ $B_z = 0.90 \mu\text{T}$	$B_x = -2.35 \mu\text{T}$ $B_z = 5.07 \mu\text{T}$	$B_x = 3.05 \mu\text{T}$ $B_z = -2.38 \mu\text{T}$	$B_x = 0.47 \mu\text{T}$ $B_z = 1.79 \mu\text{T}$
70 %	30 %	$B_x = 2.83 \mu\text{T}$ $B_z = -2.80 \mu\text{T}$	$B_x = 1.73 \mu\text{T}$ $B_z = -1.01 \mu\text{T}$	$B_x = 6.77 \mu\text{T}$ $B_z = -7.39 \mu\text{T}$	$B_x = 5.67 \mu\text{T}$ $B_z = -5.60 \mu\text{T}$
70 %	50 %	$B_x = 2.10 \mu\text{T}$ $B_z = -1.61 \mu\text{T}$	$B_x = 0.25 \mu\text{T}$ $B_z = 1.37 \mu\text{T}$	$B_x = 6.03 \mu\text{T}$ $B_z = -6.20 \mu\text{T}$	$B_x = 4.19 \mu\text{T}$ $B_z = -3.22 \mu\text{T}$
70 %	70 %	$B_x = 1.36 \mu\text{T}$ $B_z = -0.41 \mu\text{T}$	$B_x = -1.22 \mu\text{T}$ $B_z = 3.76 \mu\text{T}$	$B_x = 5.30 \mu\text{T}$ $B_z = -5.00 \mu\text{T}$	$B_x = 2.72 \mu\text{T}$ $B_z = -0.83 \mu\text{T}$

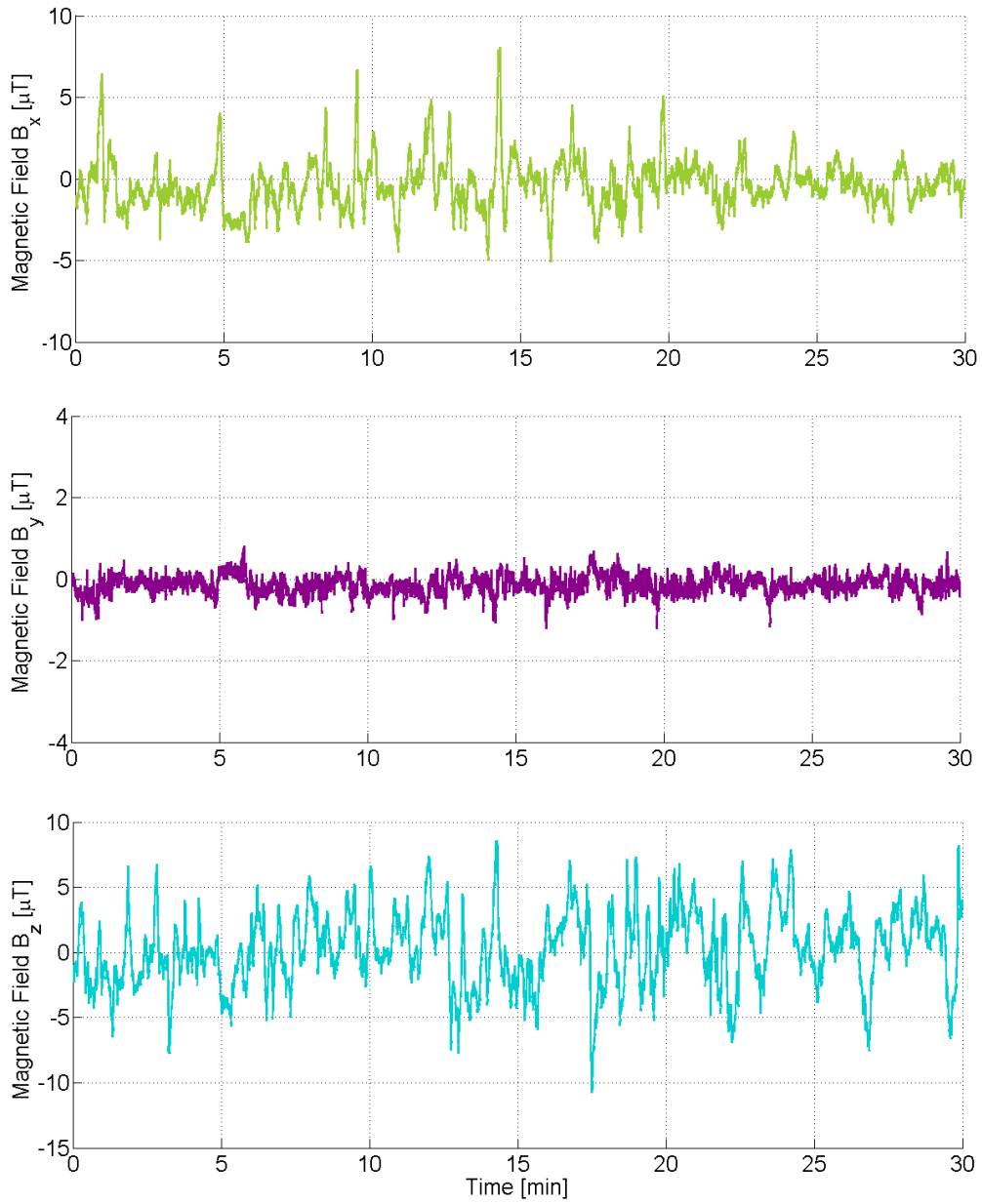


FIGURE 22 – Magnetic field created by the RER over the course of 30 minutes (without geomagnetic field) measured in the *Centre Automatique et Systèmes*

What is interesting is that these calculated values are really close to what is measurable in point P , which is similar to the monitoring point of the measurements in figure 19. However, in this case the axes of the sensor were oriented as such that the y -axis was not pointing eastwards but approximately in direction of the nearby RER line, which follows the course of the *Boulevard Saint-Michel*. The evaluated data, that is to say the magnetic field created by the RER without the geomagnetic field, is displayed in figure 22.

Even though it cannot be ruled out that this measuring is also influenced by other sources of magnetic fields, the RER accounts as a key source. This conclusion can be safely drawn from the closeness of the measurements and the calculations. As the changes are of an order of magnitude that is detectable by magnetometers, the magnetic field induced by the RER could influence algorithms using these data. This statement can easily be transferred to other direct current public inner-city transport systems.

4.2 Alternating Current Railway Systems

Some inner-city transport systems also work at alternating current, e.g. the German underground trains at 16.7 Hz. In this case, the precedingly discussed irregular, low-frequency magnetic field, whose time course depends on the motor load and the number of trains, is superimposed by the magnetic field of the alternating current. As the catenaries and the rails are approximated as straight wires, this regularly oscillating magnetic field resembles to the magnetic field of the previously discussed overhead power line. The strength of the magnetic field however is significantly lower due to the fact that the current through the overhead wires and rails are of opposite signs. The same applies for inter-city trains, which usually run at 50 Hz alternating current.

5 Conclusion

Apart from the quasi-stationary geomagnetic field, we face numerous magnetic fields in daily life. In the stationary and low-frequency domain the most important sources are : electric appliances, public electricity supply systems, such as overhead power lines and underground cables, and public transport systems. The relevance of each source essentially depends on the respective location, but especially in cities many different sources accumulate to a very noisy magnetic field. For more information see [18].

Références

- [1] A. Abart, E. Schmutzner, and M. Zambelli. EMV : niederfrequente Magnetfelder in elektrischen Netzen mit mehrfacher Rückleitung. *Elektrotechnik und Informationstechnik*, 119 :145–152, 2002.
- [2] H. Bahlburg and C. Breitkreuz. *Grundlagen der Geologie*. Spektrum Akademischer Verlag, 2012.
- [3] Bundesamt für Strahlenschutz. Elektrische und magnetische Felder der Stromversorgung, May 2012.
- [4] Bundesverband der Energie- und Wasserwirtschaft e. V. Deutsches Stromnetz ist 1.78 Millionen Kilometer lang. Press release, 2011 March.
- [5] U. Christensen and A. Tilgner. Der Geodynamo. *Physik Journal*, 10 :41–47, 2002.

- [6] G. Coget and M. Olivier. Le matériel d'interconnexion SNCF/RATP MI79. *Revue générale des chemins de fer*, January, 1982.
- [7] Electricité Réseau Distribution France. Rapport d'activité et de développement durable 2011, 2011.
- [8] L. Fendrich, editor. *Handbuch der Eisenbahninfrastruktur*. Springer Verlag, 2007.
- [9] P. Follenfant and J.-P. Leteurtrous. Rapport sur la maîtrise de l'urbanisme autour des lignes de transport d'électricité. Technical report, Ministère de l'Économie de l'Industrie et de l'Emploi, 2010.
- [10] R. F. Hüttl. *Ein Planet voller Überraschungen/Our Surprising Planet*. Spektrum Akademischer Verlag, 2011.
- [11] F. Jarrier. Railway maps of urban transports. Website, 2011. <http://carto.metro.free.fr> (accessed December 5, 2012).
- [12] B. Klose. *Meteorologie*. Springer Verlag, 2008.
- [13] B. Oswald. Skript Freileitungen. Technical report, Institut für Energieversorgung und Hochspannungstechnik, Universität Hannover, 2005.
- [14] A. Price. Daily variations of the geomagnetic field. *Space Science Review*, 9 :151–197, 1969.
- [15] D. Redoutey. *Le matériel moteur de la SNCF*. La vie du Rail, 2007.
- [16] Régie Autonome des Transports Parisiens. Horaires RER. Website, 2012. <http://www.ratp.fr/horaires/fr/ratp/rer> (accessed December 5, 2012).
- [17] Réseau de Transport d'Electricité. Bilan électrique 2011, 2011.
- [18] A. Schwab and W. Kürner. *Elektromagnetische Verträglichkeit*. Springer Verlag, 2011.
- [19] J. Silny. Elektromagnetische Felder im Alltag. Technical report, Landesanstalt für Umweltschutz Baden-Württemberg, Forschungszentrum für Elektromagnetische Verträglichkeit RWTH Aachen, 2002.
- [20] Xsens-Technologies B.V. *Motion tracker B Technical Documentation*, 1.01 edition, 2002-2003.

A Nomenclature

A.1 Vectors and Matrices

\mathbf{A}	state matrix (state space)
\mathbf{B}	magnetic field vector in R_i
$\nabla \mathbf{B} = \frac{\partial \mathbf{B}}{\partial \mathbf{X}}$	Jacobian matrix of the magnetic field \mathbf{B}
\mathbf{b}	magnetic field vector in R_b
$\hat{\mathbf{b}}$	estimation of the magnetic field vector \mathbf{b}
$\nabla \mathbf{b} = \frac{\partial \mathbf{b}}{\partial \mathbf{x}}$	Jacobian matrix of the magnetic field \mathbf{b}
\mathbf{C}	output matrix (state space)
\mathbf{D}	electric flux density
\mathbf{E}	electric field (strength)
\mathbf{e}	unit vector
$\mathbf{e}_X, \mathbf{e}_Y, \mathbf{e}_Z$	basis vectors of the inertial frame of reference
$\mathbf{e}_x, \mathbf{e}_y, \mathbf{e}_z$	basis vectors of the body frame of reference

F_E	external forces
H	magnetic field strength
J	current density
L	gain matrix
m	magnetic dipole moment
p, q	coordinate vectors
Q_B	observability matrix
R	rotation matrix
R_b	matrix containing the basis vectors of the body reference frame
R_i	matrix containing the basis vectors of the inertial reference frame
R_x, R_y, R_z	rotation matrices about the x-,y- and z-axis
r	distance vector
$T_{i \rightarrow b}$	transformation matrix between R_i and R_b
V	velocity vector in R_i
\hat{V}	estimation-based calculation of the velocity vector V
v	velocity vector in R_b
\hat{v}	estimation of the velocity vector v
W	rate of turn vector in R_i
w	rate of turn vector in R_b
X	position vector in R_i
\hat{X}	estimation-based calculation of the position vector X
x	position vector in R_b
y	output vector (state space)
β	magnetic field vector
ν	velocity vector
ξ	position vector
Υ	linear transposition matrix (arbitrary)
χ	state vector
$\tilde{\chi}$	alternative state vector
Ω_W	rotation matrix corresponding to the rate of turn vector W
Ω_w	rotation matrix corresponding to the rate of turn vector w
ω	rate of turn vector

A.2 Scalars, Functions and Sets

B_x, B_y, B_z	coordinates of B , the magnetic field vector in R_i
b_x, b_y, b_z	coordinates of b , the magnetic field vector in R_b
$\hat{b}_x, \hat{b}_y, \hat{b}_z$	coordinates of \hat{b} , the estimated magnetic field vector
C	substation charge
f	frequency
f	analytic function
h	auxiliary function
I	current
k	wave number
L	motor load
l	length
l_1, l_2	constant gains of the gain matrix L
M	magnetic dipole moment (absolute value)
n, m	quantities

P, Q, R	coordinates of \mathbf{W} , the rate of turn vector in R_i
p, q, r	coordinates of \mathbf{w} , the rate of turn vector in R_b
r	distance
\mathfrak{R}_b	body reference frame
R_b	basis of the body reference frame
\mathfrak{R}_i	inertial reference frame
R_i	basis of the inertial reference frame
t	time
t_0	start time
Δt	discrete time step, reciprocal of the sample frequency
U, V, W	coordinates of \mathbf{V} , the velocity vector in R_i
$\hat{U}, \hat{V}, \hat{W}$	coordinates of $\hat{\mathbf{V}}$, the estimation-based calculation of the velocity vector in R_i
u, v, w	coordinates of \mathbf{v} , the velocity vector in R_b
$\hat{u}, \hat{v}, \hat{w}$	coordinates of $\hat{\mathbf{v}}$, the estimated velocity vector in R_b
V	Lyapunov candidate function
X, Y, Z	coordinates of \mathbf{X} , the position vector in R_i
$\hat{X}, \hat{Y}, \hat{Z}$	coordinates of $\hat{\mathbf{X}}$, the estimation-based calculation of the position vector in R_i
x, y, z	coordinates of \mathbf{x} , the position vector in R_b
x, y, z	Cartesian coordinates
α	auxiliary angle
ε_0	electric constant
ε_r	relative electric permittivity
μ_0	magnetic constant
μ_r	relative magnetic permeability
ρ	volume charge density
φ	angle of the right triangle defined by the Cartesian coordinates x (opposite leg) and z (adjacent leg)
$\Delta\varphi$	phase shift
ϕ, θ, ψ	set of angles describing a rotational state
ω	angular velocity

A.3 Indices

<i>avg</i>	average
<i>b</i>	body
<i>cat</i>	catenary
<i>dip</i>	dipole
<i>dir</i>	direction
<i>e</i>	estimation
<i>eff</i>	effective
<i>f</i>	final
<i>gyro</i>	gyrometer
<i>I</i>	current
<i>i</i>	inertial
<i>j, k</i>	counter variable
<i>m</i>	measured
<i>magneto</i>	magnetometer
<i>max</i>	maximum
<i>min</i>	minimum

<i>MV</i>	mean value
<i>p</i>	prediction
<i>r</i>	distance
<i>s</i>	sensor
<i>sp</i>	sample
<i>stat</i>	stationary
<i>t</i>	trains
<i>trans</i>	transient
<i>w</i>	wire
<i>X, Y, Z</i>	component in <i>X</i> -, <i>Y</i> - and <i>Z</i> -axis direction
<i>x, y, z</i>	component in <i>x</i> -, <i>y</i> - and <i>z</i> -axis direction

A.4 List of Abbreviations

AC	Alternating Current
AWGN	Additive White Gaussian Noise
CAS	<i>Centre Automatique et Systèmes</i>
DC	Direct Current
IRT	<i>Institut für Regelungstechnik</i>
PSU	Power Supply Unit
RATP	<i>Régie Autonome des Transports Parisiens</i>
RER	<i>Réseau Express Régionale</i>
RMS	Root Mean Square
SNCF	<i>Société Nationale des Chemins de Fer Français</i>